Low-energy kaon-nuclei interaction studies by AMADEUS

Kristian Piscicchia[1,2*]

[1] Centro Ricerche Enrico Fermi - Museo Storico della Fisica e Centro Studi e Ricerche "Enrico Fermi", 00184 Roma, Italy

[2] INFN Laboratori Nazionali di Frascati, 00044 Frascati, Italy

On the behalf of the AMADEUS collaboration

14th International Conference on Hypernuclear and Strange Particle Physics - HYP2022

27 June -1 July 2022, Prague

***kristian.piscicchia@cref.it**

K⁻p scattering amplitude

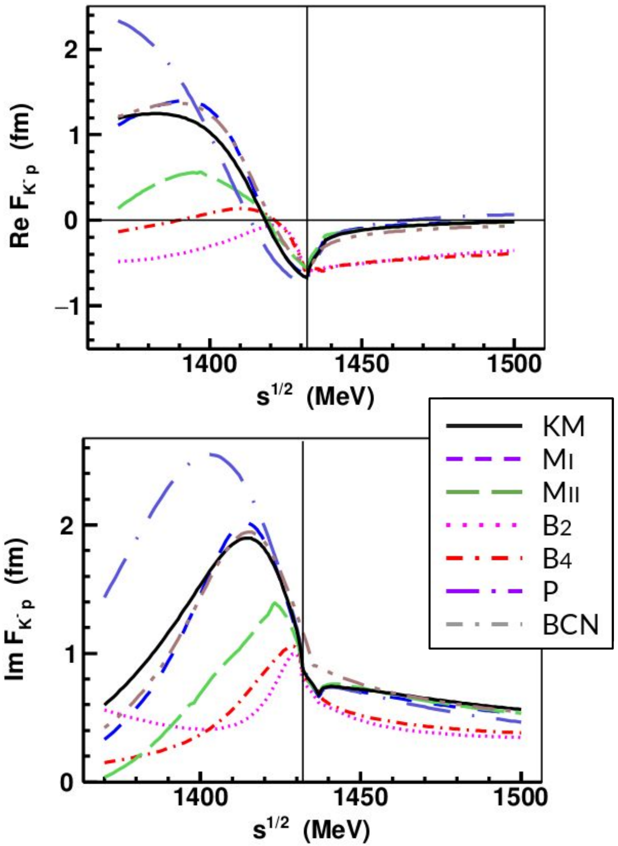

K^-p scattering amplitude in Chiral calculations

- Kyoto-Munich (KM)

  Y. Ikeda, T. Hyodo, W. Weise, Nucl. Phys. A 881 (2012) 98
- Murcia (MI , MII)

  Z. H. Guo, J. A. Oller, Phys. Rev. C 87 (2013) 035202
- Bonn (B2 , B4)

  M. Mai, U.-G. Meißner - Eur. Phys. J. A 51 (2015) 30
- Prague (P)

  A. Cieply, J. Smejkal, Nucl. Phys. A 881 (2012) 115
- Barcelona (BCN)

  A. Feijoo, V. Magas, À. Ramos, Phys. Rev. C 99 (2019) 035211

A. Cieply, J. Hrtánková, J. Mareš, E. Friedman, A. Gal and A. Ramos, AIP Conf. Proc. 2249, no.1, 030014 (2020).

Experimental constraints at K̄N threshold

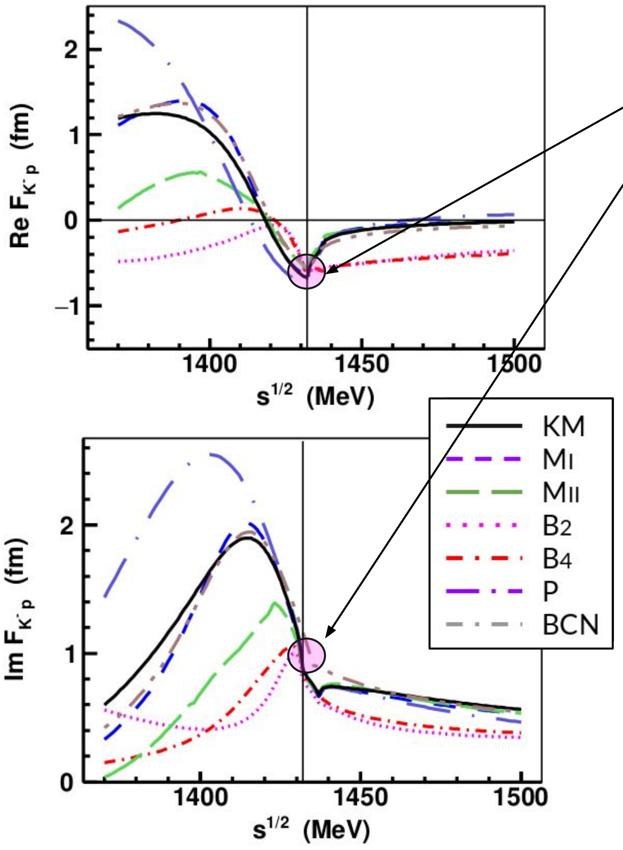

Precise SIDDHARTA measurement of kaonic hydrogen 1s level shift and width

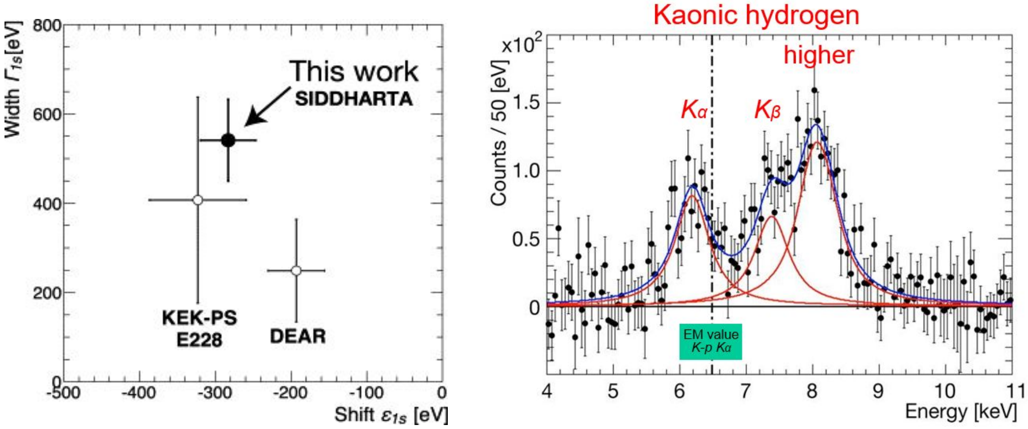

M. Bazzi et al.. 2011. (SIDDHARTA Coll.), Phys. Lett. B704, 113

$$\Delta E_N(1s) = 283 \pm 36(stat.) \pm 6(syst.)\ \text{eV}$$

$$\Gamma(1s) = 541 \pm 89(stat.) \pm 22(syst.)\ \text{eV}$$

$$\varepsilon + \frac{i\Gamma}{2} = 2\alpha^3\mu^2 a_{K^-p} = 412\,\tfrac{eV}{fm}\, a_{K^-p}$$

K^-p scattering amplitude

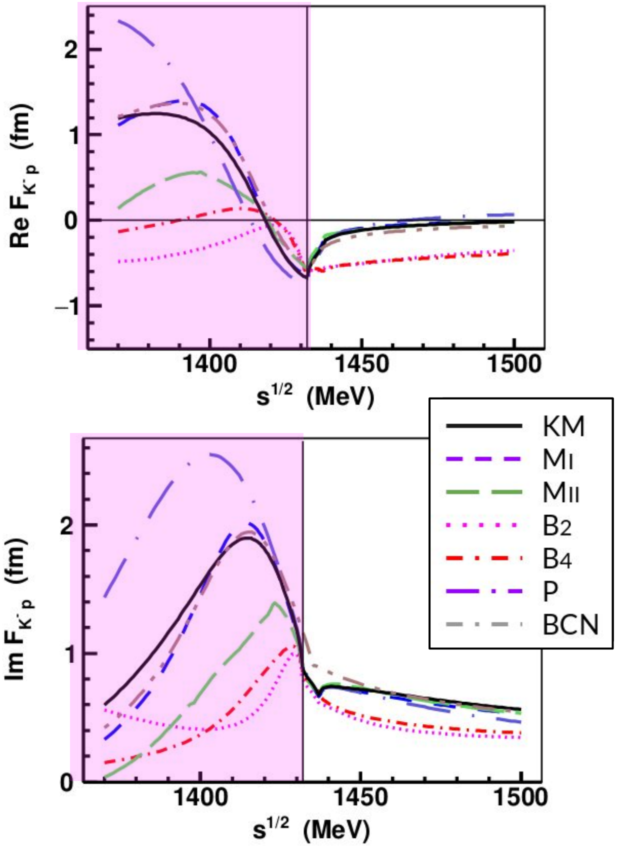

K^-p scattering amplitude in Chiral calculations

- Kyoto-Munich (KM)

  Y. Ikeda, T. Hyodo, W. Weise, Nucl. Phys. A 881 (2012) 98
- Murcia (MI , MII)

  Z. H. Guo, J. A. Oller, Phys. Rev. C 87 (2013) 035202
- Bonn (B2 , B4)

  M. Mai, U.-G. Meißner - Eur. Phys. J. A 51 (2015) 30
- Prague (P)

  A. Cieply, J. Smejkal, Nucl. Phys. A 881 (2012) 115
- Barcelona (BCN)

  A. Feijoo, V. Magas, À. Ramos, Phys. Rev. C 99 (2019) 035211

Large discrepancies in the region below threshold!

What above the threshold?

K-p inelastic low-energy cross sections

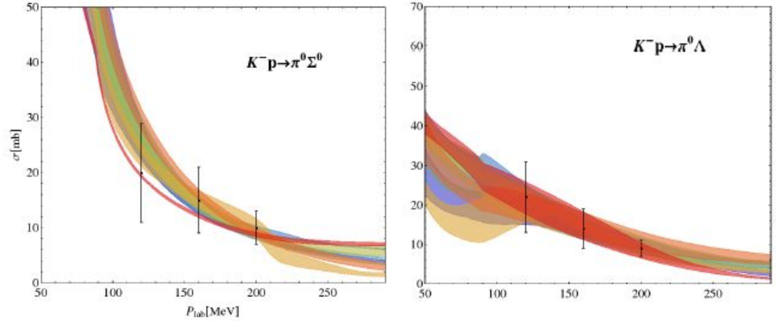

M. Mai and U. G. Meissner, Eur. Phys. J. A 51, 30 (2015).

Phen. [Y. Ikeda and T. Sato, Phys. Rev. C76, 035203 (2007)]

Chiral [S. Ohnishi, Y. Ikeda, T. Hyodo, W. Weise, Phys.Rev. C93 (2016) no.2, 025207]

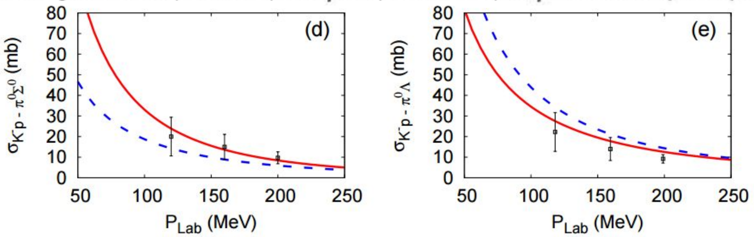

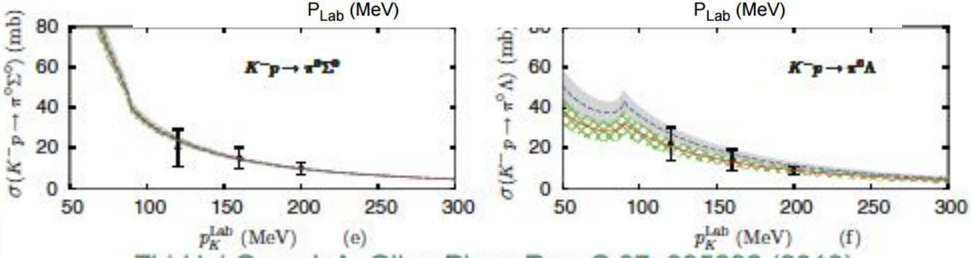

Zhi-Hui Guo, J. A. Oller, Phys. Rev. C 87, 035202 (2013).

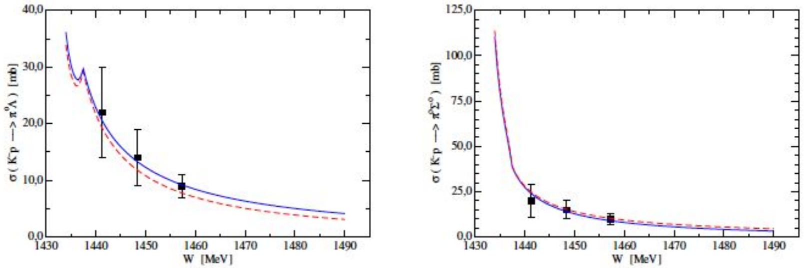

P.C. Bruns, A. Cieply, Nucl. Phys. A 1019, (2022) 122378.

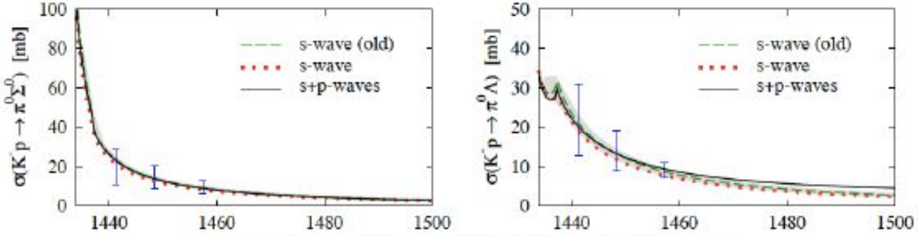

A. F., D. Gazda, V. Magas, A. Ramos, Symmetry 13 (2021) 8, 1434

What above the threshold?

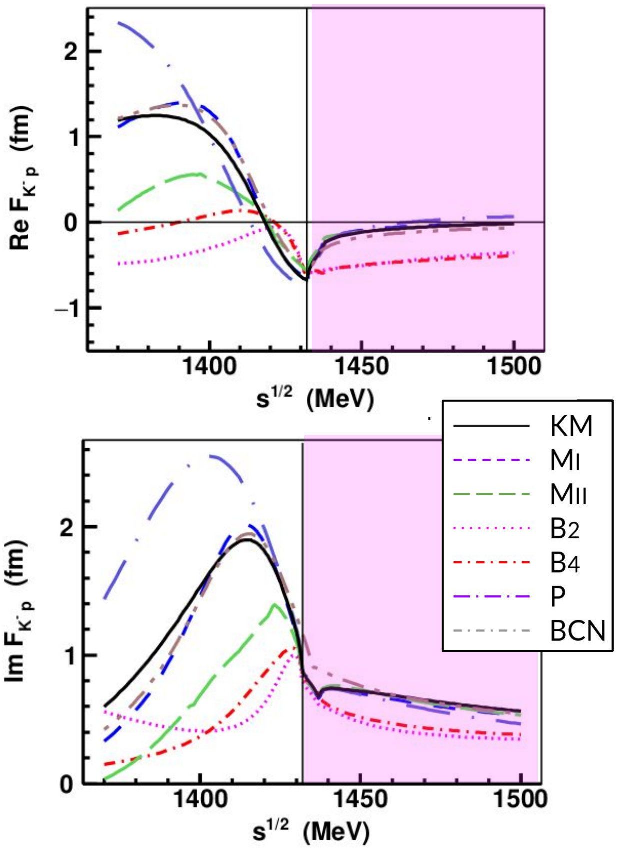

K-p elastic and inelastic low-energy cross sections

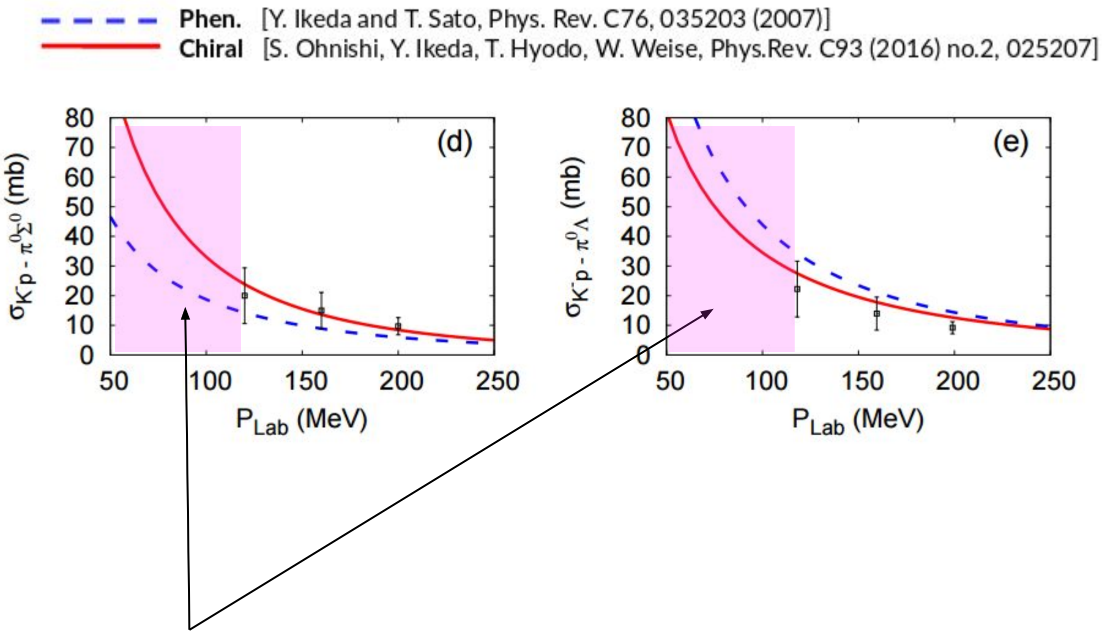

lack of data for p_K < 120 MeV/c

AMADEUS can give this info

K^-n scattering amplitude below threshold

A. Cieply, J. Hrtánková, J. Mareš, E. Friedman, A. Gal and A. Ramos, AIP Conf. Proc. 2249, no.1, 030014 (2020).

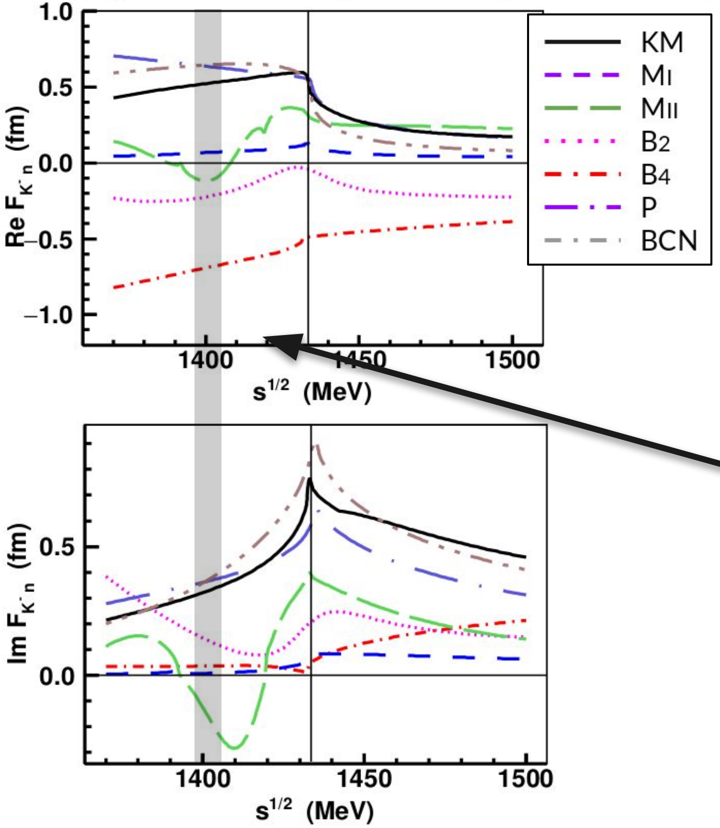

K^-n scattering amplitude (s-wave)

even larger spread in I=1 channel

Experimental information was missing:

- **SIDDHARTA-2** → **first experimental constraint at threshold**

- **AMADEUS** → **determination of the non-resonant (s-wave) transition amplitude below threshold**

  Investigated using:

  K^- "n" → $\Lambda\pi^-$ to extract $|f^{N-R}_{\Lambda\pi}(I=1)|$

  with bound neutron in ^{4}He

AMADEUS scientific case

AMADEUS (**A**ntikaonic **M**atter **A**t **DAΦNE**: an **E**xperiment with **U**nravelling **S**pectroscopy) investigates **low-energy K^- absorption in nuclei** with the aim to extract information on:

- K^-N interaction above and below threshold
  - Λ(1405) nature
  - K^-N scattering amplitudes and cross sections
- K^-NN, K^-NNN, K^-NNNN (multi-nucleon) interactions
  - K^--multi nucleon cross sections
  - essential for the determination of K^--nuclei optical potential
  - kaonic bound states
- Hyperon-nucleon/(multi-nucleons) interaction cross sections

DAΦNE the Φ factory

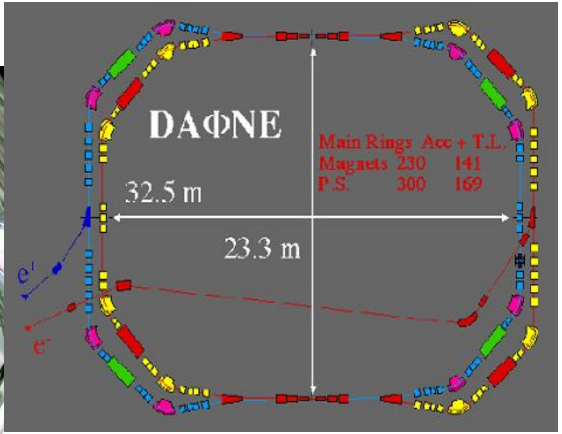

- $e^+ e^-$ at 510 MeV
- φ resonance decays at 49.2 % in $K^+ K^-$ back to back pair
- Very low momentum (≈ 127 MeV) K^- beam

Fantastic low momentum K^- factory

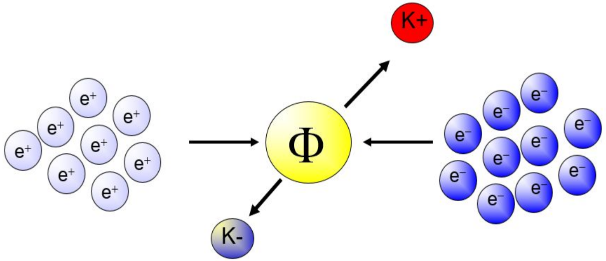

Suitable for low-energy kaon physics:
→ **Kaonic atoms** (**SIDDHARTA-2**)
→ **Kaon-nucleons/nuclei interaction** studies (**AMADEUS**)

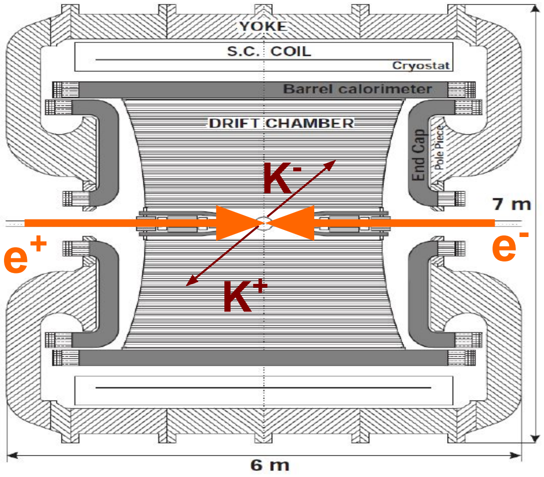

The KLOE detector

Cylindrical drift chamber with a **4π geometry** and electromagnetic calorimeter, **96% acceptance**

- optimized in the energy range of all **charged particles** involved
- **good performance** in detecting **photons and neutrons** checked by kloNe group
  [M. Anelli et al., Nucl Inst. Meth. A 581, 368 (2007)]

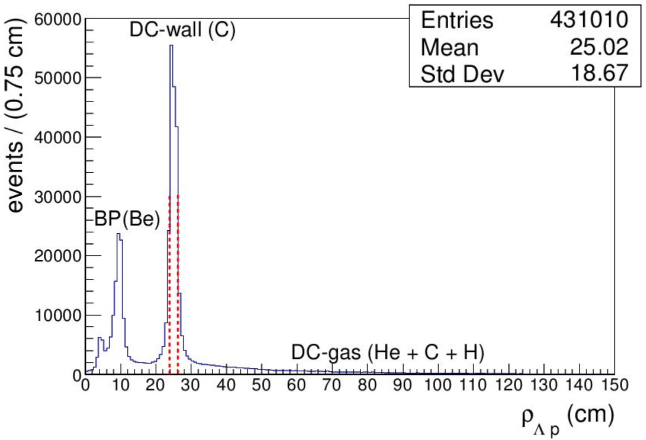

KLOE used as an active target

- DC wall (750 μm C foil , 150 μm Al foil);
- DC gas (90% He, 10% C_4H_{10}).
  +
  pure sample of K^- ^{12}C absorptions at-rest

K^- absorptions at-rest and in-flight

AT-REST

K^- absorbed from atomic orbitals

(p_K ~ 0 MeV/c)

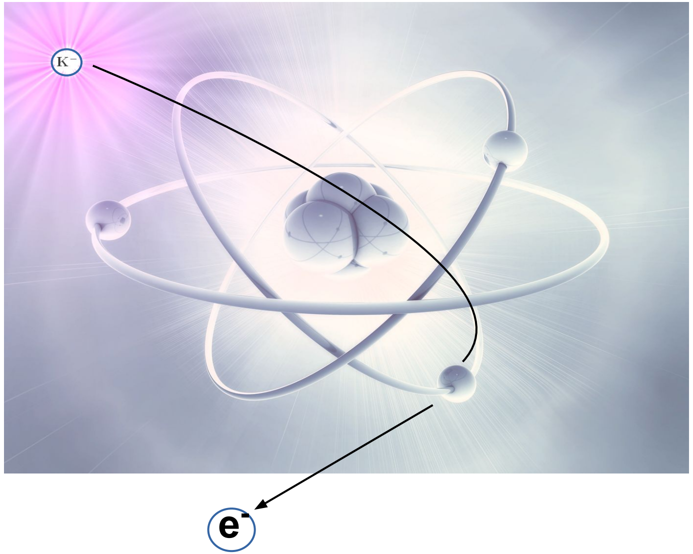

IN-FLIGHT

(p_K~ 100 MeV/c)

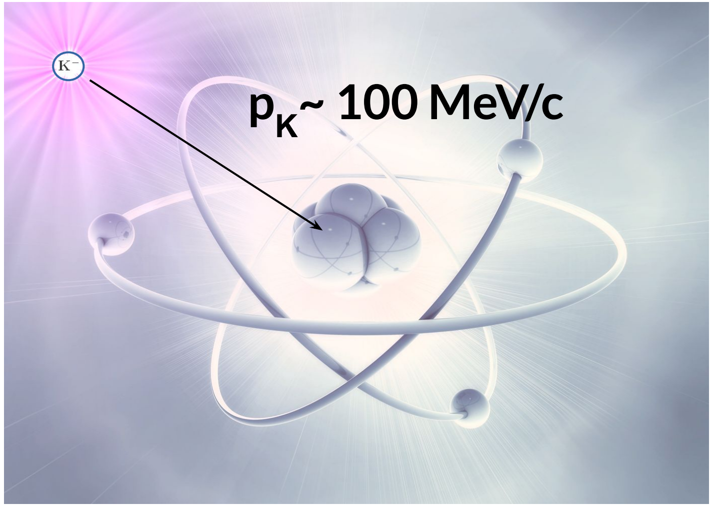

K- n → Λπ⁻ events selection and interpretation

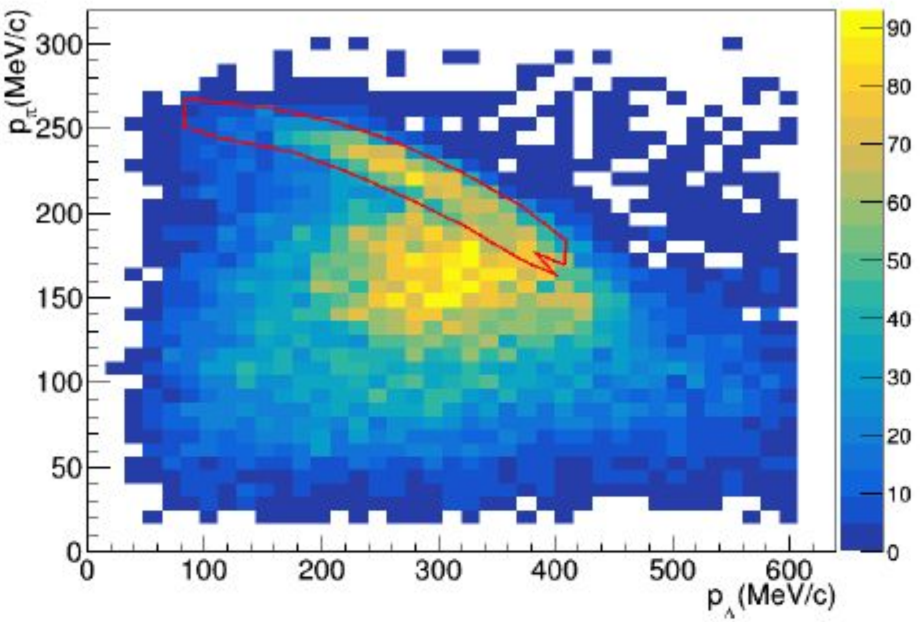

FIG. 2. (Color online) Experimental distribution of the π^- vs Λ momenta. The red line represents the selection of the direct $\Lambda\pi^-$ production events. See the text for details.

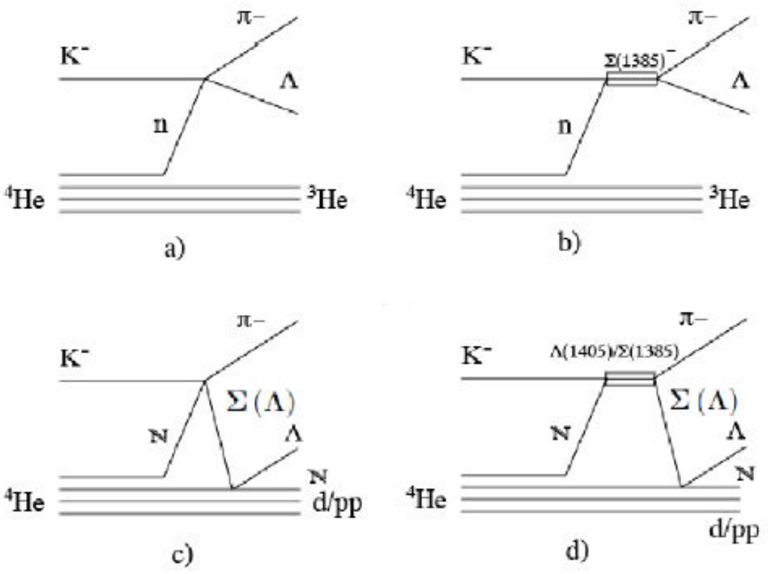

FIG. 1. Panels a) and b) show the non-resonant and resonant $\Lambda\pi^-$ direct productions, respectively. Panels c) and d) show the primary hyperon-pion formation, followed by the inelastic/elastic scattering of the Σ/Λ hyperon on a single nucleon, for the resonant and non-resonant cases, respectively.

Events selection - $\Lambda \rightarrow p\,\pi^-$ (BR = 63.9 ± 0.5%)

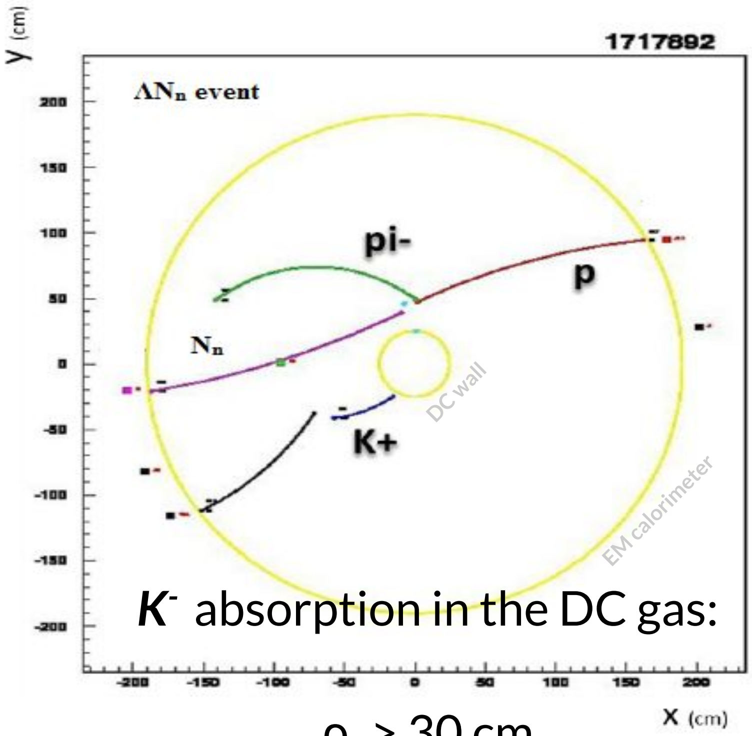

K$^-$ absorption in the DC gas:

$\rho_\Lambda > 30$ cm

contamination with ***K***$^-$ absorption in the DC wall < 3%

Opposite charged tracks with common vertex,

main background: $(K^\pm \rightarrow \pi^\pm \pi^\pm \pi^\mp)$

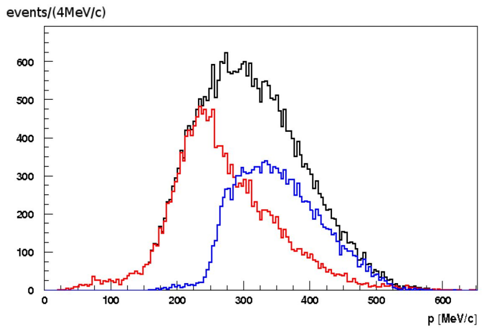

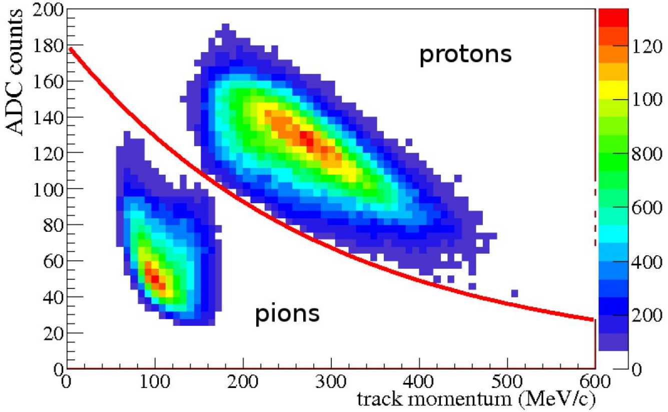

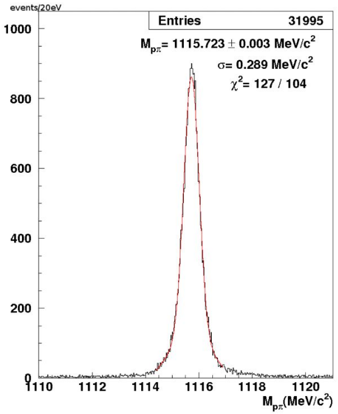

Simultaneous fit : $p_{\Lambda\pi^-}$ - $m_{\Lambda\pi^-}$ - $\cos\theta_{\Lambda\pi^-}$

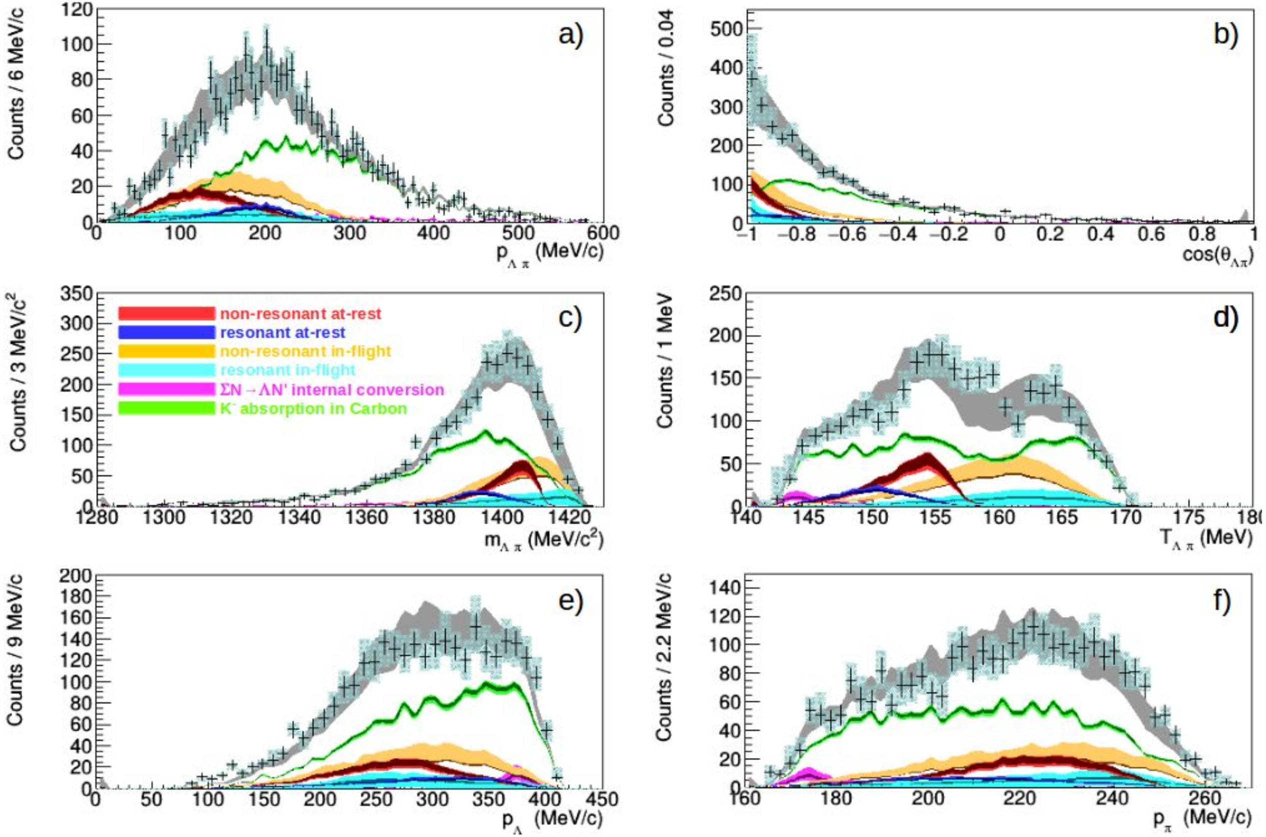

Investigated using:

K^- "**n**" $^3He \rightarrow \Lambda\pi^- \, ^3He$

$$E_{Kn} \sim -B_n - < \frac{p^2_{\Lambda\pi}}{2\mu_{\pi,\Lambda,3He}} >$$

33 ± 6 MeV below threshold

see also

A. Cieply et al., Phys. Lett. B 702 (2011) 402
T. Hoshino et al., Phys. Rev. C 96 (2017) 045204
N. Barnea, E. Friedman,
A. Gal, Nucl. Phys. A968 (2017)

[K. Piscicchia, S. Wycech, L. Fabbietti et al. Phys.Lett. B782 (2018) 339-345]
[K. Piscicchia, S. Wycech, C. Curceanu, Nucl. Phys. A 954 (2016) 75-93]

Outcome of the measurement

Investigated using:

K^- "n" ^{3}He → $\Lambda\pi^-$ ^{3}He

Energy of the K^-n system:

$$E_{Kn} \sim -B_n - < \frac{p^2_{\Lambda\pi}}{2\mu_{\pi,\Lambda,3He}} >$$

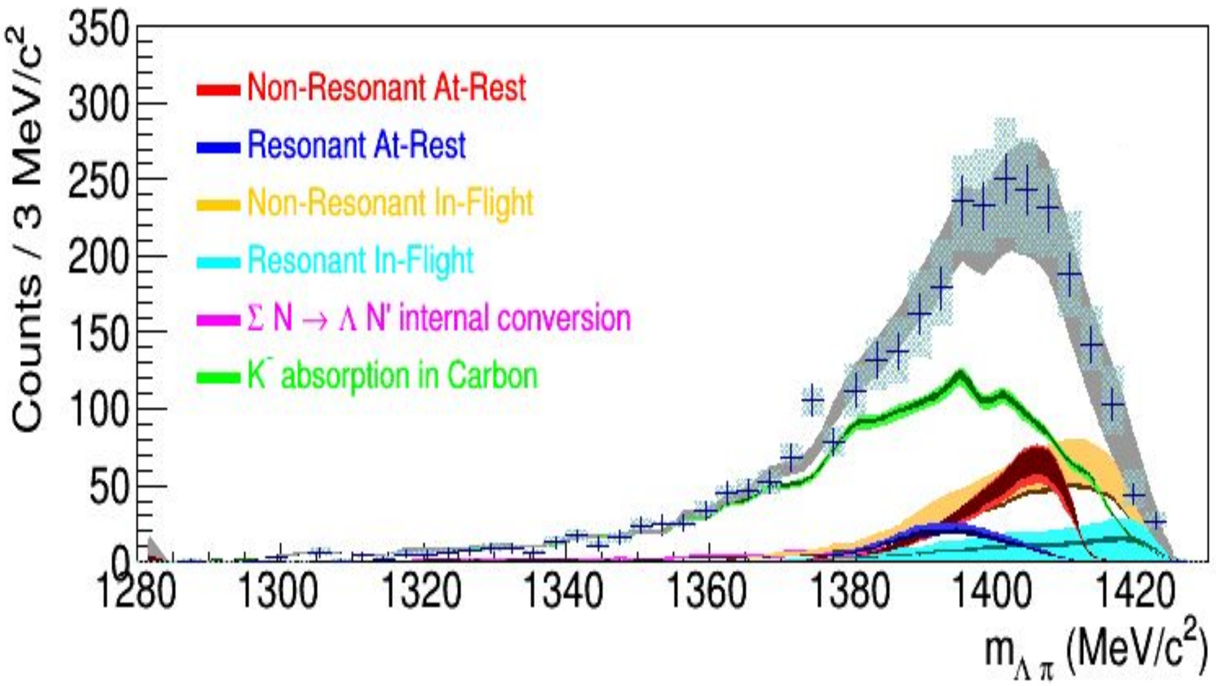

[K. Piscicchia, S. Wycech, L. Fabbietti et al. Phys.Lett. B782 (2018) 339-345]
[K. Piscicchia, S. Wycech, C. Curceanu, Nucl. Phys. A 954 (2016) 75-93]

Outcome of the measurement

Investigated using: **K⁻ "n"** ^{3}He → **Λπ⁻** ^{3}He

$$|f_{ar}^{nr}| = (0.334 \pm 0.018\,\mathrm{stat}^{+0.034}_{-0.058}\mathrm{syst})\ \mathrm{fm}$$

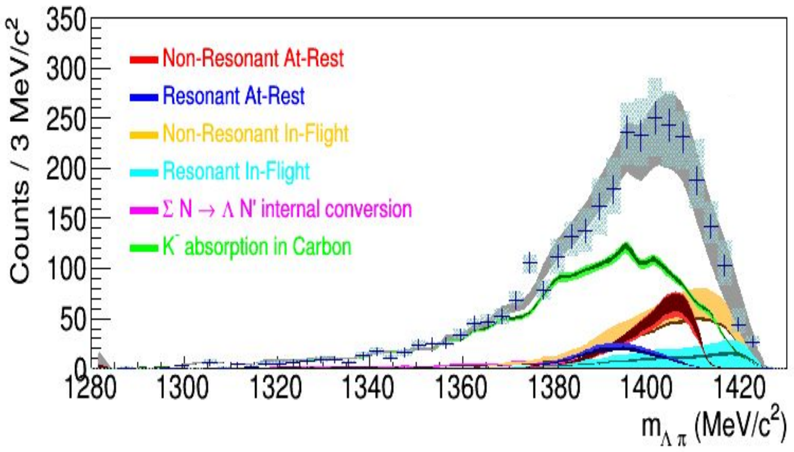

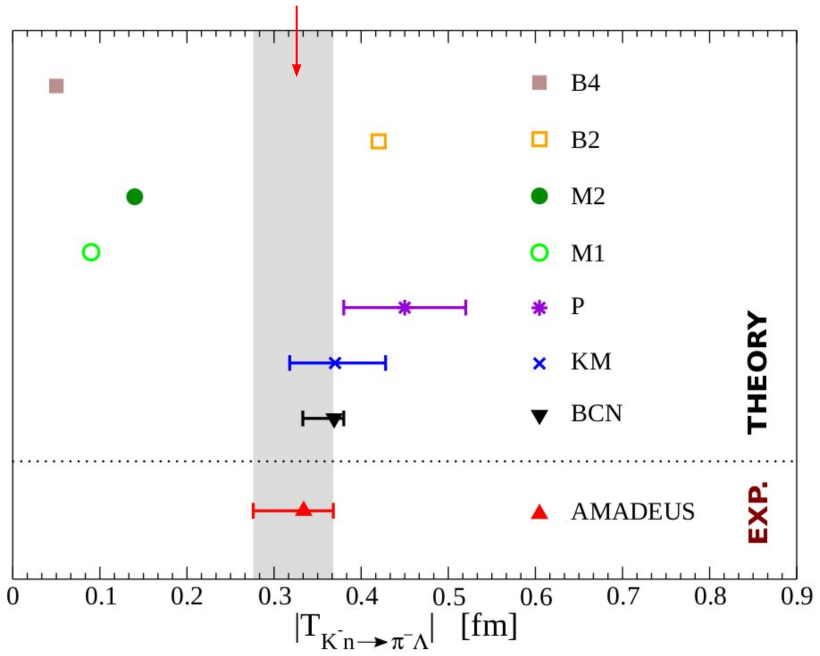

[K. Piscicchia, S. Wycech, L. Fabbietti et al. Phys.Lett. B782 (2018) 339-345]
[K. Piscicchia, S. Wycech, C. Curceanu, Nucl. Phys. A 954 (2016) 75-93]

Simultaneous measurement of the

$K p \rightarrow \Sigma^0 \pi^0$ & $\Lambda \pi^0$

cross sections at $p_{K-} = 98 \pm 10$ MeV/c

Events selection - γ_1, γ_2 & γ_3

$$K^{-}\text{"}p\text{"} \rightarrow \Sigma^0\pi^0 \rightarrow (\Lambda\gamma_3)\,(\gamma_1\gamma_2) \rightarrow (p\pi^-)\gamma_1\gamma_2\gamma_3$$

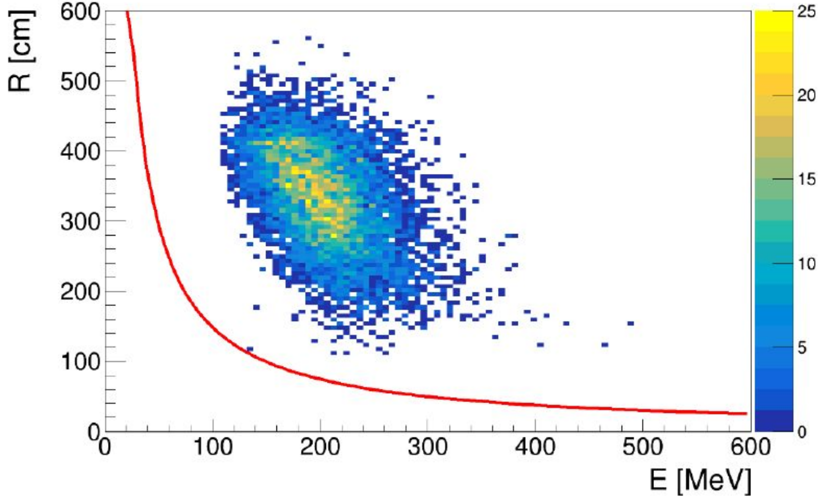

- $K^+ \rightarrow \pi^+\pi^0$ background is rejected

- three photon clusters are selected by TOF

$$\chi^2_t = t^T\, V_t^{-1}\, t$$

with $t = t_i - t_j$; $t_i = t_{cli} - r_i/c$

- disentangling γ_1, γ_2 & γ_3 :

$$\chi^2_{\pi\Sigma} = \frac{(m_{\pi^0} - m_{ij})^2}{\sigma^2_{ij}} + \frac{(m_{\Sigma^0} - m_{k\Lambda})^2}{\sigma^2_{k\Lambda}}$$

- MC based rejection criteria:

$$\chi^2_t \leq 20,\ \chi^2_{m_{\gamma_1\gamma_2}} \leq 5 \text{ and } \chi^2_{m_{\Lambda\gamma_3}} \leq 4$$

- Cluster splitting background free! Algorithm overall efficiency for γ detection: $0.98 \pm 0.01.$

Events selection - Σ^0 & π^0

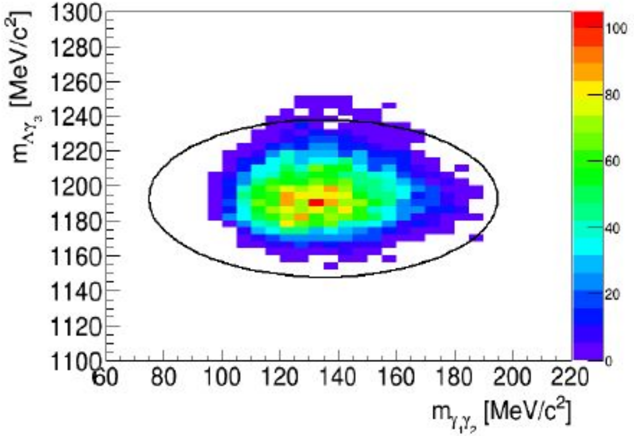

FIG. 1. The plot shows the $m_{\Lambda\gamma_3}$ distribution as a function of $m_{\gamma_1\gamma_2}$. A black ellipse represents the applied selection in the two invariant masses space.

$$\frac{\left(m_{\Lambda\gamma_3} - m_{\Sigma^0}\right)^2}{(3\sigma_{\Lambda\gamma_3})^2} + \frac{\left(m_{\gamma_1\gamma_2} - m_{\pi^0}\right)^2}{(3\sigma_{\gamma_1\gamma_2})^2} < 1$$

- RESOLUTIONS:

$\sigma_{\Lambda\gamma_3}$ ~15 MeV/c and $\sigma_{\gamma_1\gamma_2}$ ~20 MeV/c

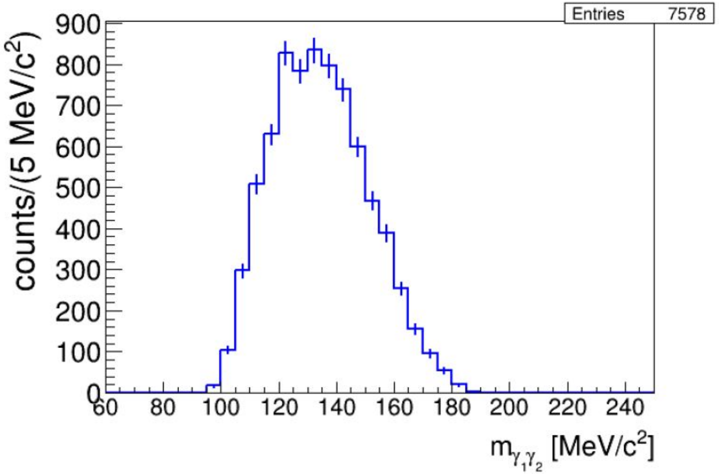

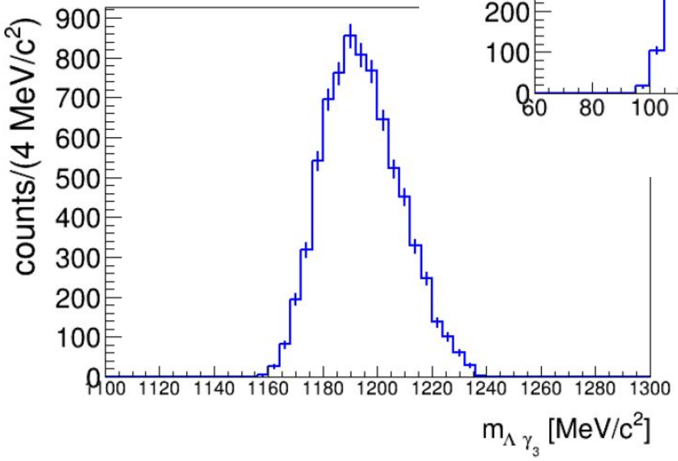

Events selection - K^- H abs. in flight

- **SIGNAL**: K^- H -> $(\Sigma^0 / \Lambda)\ \pi^0$ (*if*)

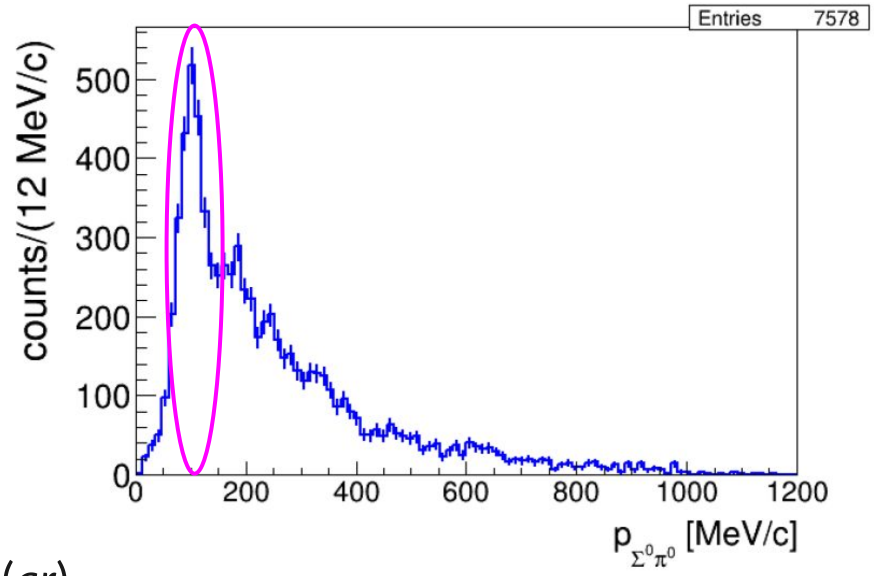

- **BACKGROUND**: K^- H -> $(\Sigma^0 / \Lambda)\ \pi^0$ (*ar*)
  K^- $(^4He/^{12}C)$ -> $(\Sigma^0 / \Lambda)\ \pi^0$ + Residual (*ar* + *if*)
  elastic or inelastic FSI of the hyperon (Y) and/or the π^0

- **FURTHERMORE** in $\Lambda\pi^0$ the direct production is affected by the background: $\Sigma^0\ \pi^0$ primary production followed by $\Sigma^0 \rightarrow \Lambda\gamma$ for ALL the channels

Events selection - K^- H abs. in flight

- **SIGNAL**: K^- H -> $(\Sigma^0 / \Lambda)\ \pi^0$ (*if*)

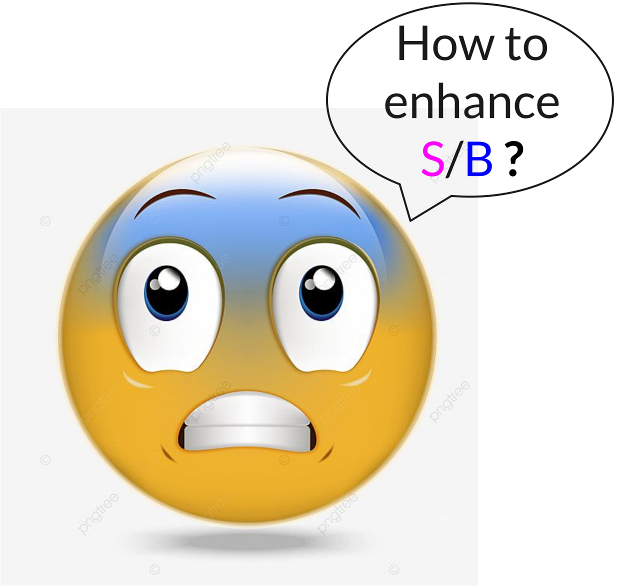

- **BACKGROUND**: K^- H -> $(\Sigma^0 / \Lambda)\ \pi^0$ (*ar*)
  K^- $(^4He/^{12}C)$ -> $(\Sigma^0 / \Lambda)\ \pi^0$ + Residual (*ar + if*)
  elastic or inelastic FSI of the hyperon (Y) and/or the π^0

- **FURTHERMORE** in $\Lambda\pi^0$ the direct production is affected by the background: $\Sigma^0\ \pi^0$ primary production followed by $\Sigma^0 \to \Lambda\gamma$ <u>for ALL the channels</u>

Events selection - K⁻ H abs. in flight

SIGNAL: $K^- H \rightarrow (\Sigma^0 / \Lambda)\ \pi^0$ (*if*)
characteristic features:

a) the kinematics (for both ar & if)
is completely determined by E-p cons.
signal is almost back to back,

b) $K^- H \rightarrow \Lambda\ \pi^0$ (*ar* & *if*) events can be sampled exploiting the resolution on p_Λ

$$\sigma_{p\Lambda} = 1.9 \pm 0.2\ \text{MeV/c}$$

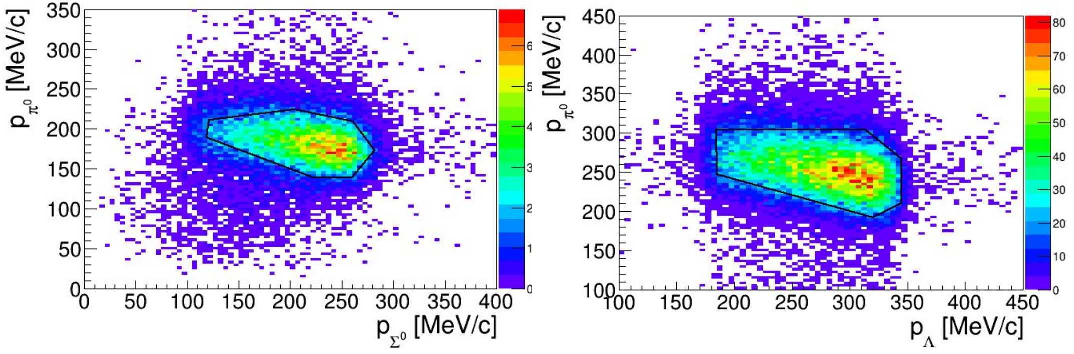

FIG. 2. The plot shows reconstructed MC p_{π^0} vs. p_Y distributions for the K^- H $\rightarrow \Sigma^0 \pi^0$ *if* reaction (top) and K^- H $\rightarrow \Lambda \pi^0$ *if* reaction (bottom). The phase space selections are represented as black contours.

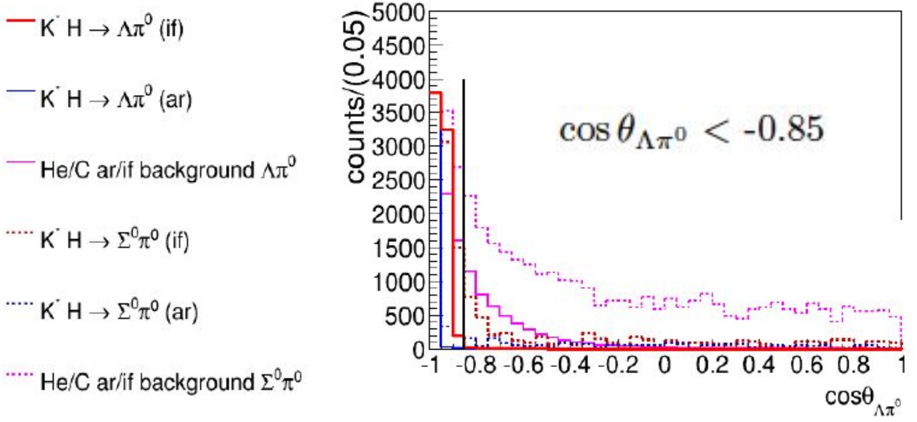

Events selection - K^- H abs. in flight

c) due to E-p cons. the total $Y\pi^0$ momentum distribution for K^- H -> Y π^0 (*if*) events reflects the original K^- momentum spectrum

FSI is negligible after phase-space selections, is considered in systematics.

residual bkg: K^- H (*ar*) and K^- ($^4He/^{12}C$) can be efficiently disentangled by means of a simultaneous fit

arbitrary normalization

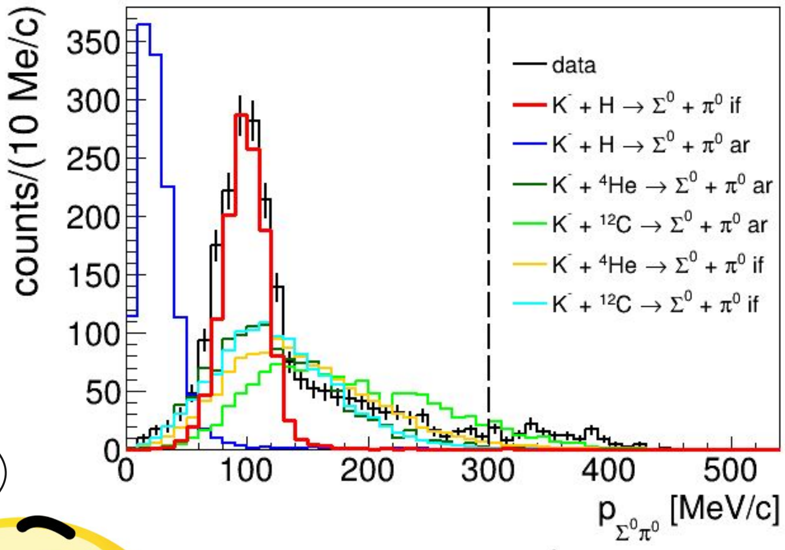

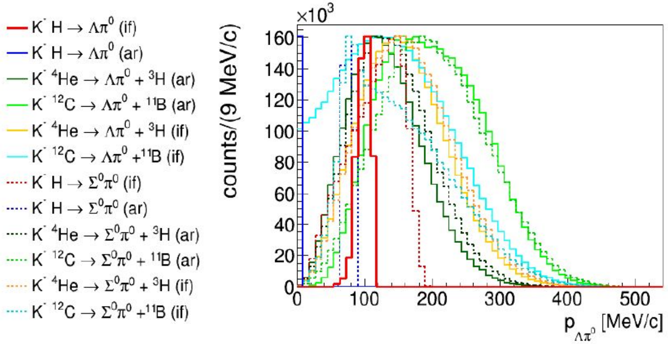

Simultaneous fit and cross sections ($\Sigma^0 \pi^0$)

$$\chi^2 = \sum_q \sum_{n=1}^{N^q_{bins}} \frac{(N^q_n - \mathcal{F}^q(q_n))^2}{\sigma^{q2}_n} \quad \text{with} \quad \mathcal{F}^q(q_n) = \sum_{i=1}^{N_{par}} \alpha_i \cdot h^q_i(q_n)$$

physical processes:

1. $K^- H \rightarrow (\Sigma^0/\Lambda)\,\pi^0\ if$ (red),
2. $K^- H \rightarrow (\Sigma^0/\Lambda)\,\pi^0\ ar$ (blue),
3. $K^- + {}^4He/{}^{12}C \rightarrow \Sigma^0/\Lambda + \pi^0 + {}^3H/{}^{11}B$ (magenta).

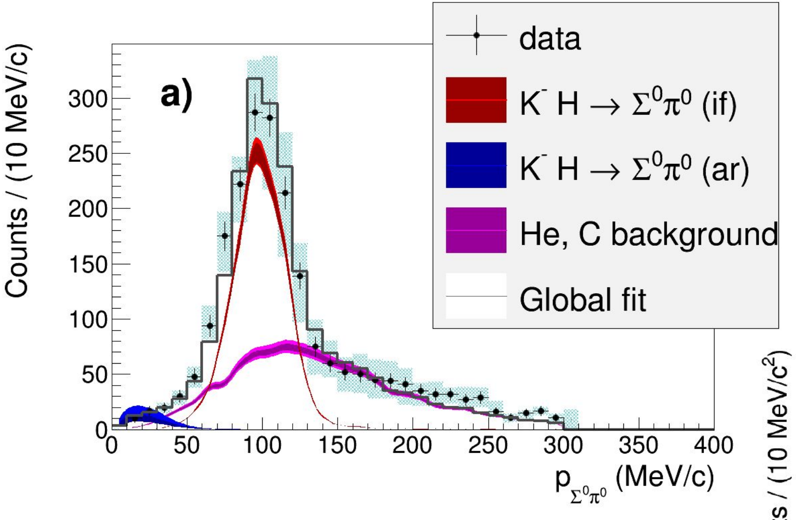

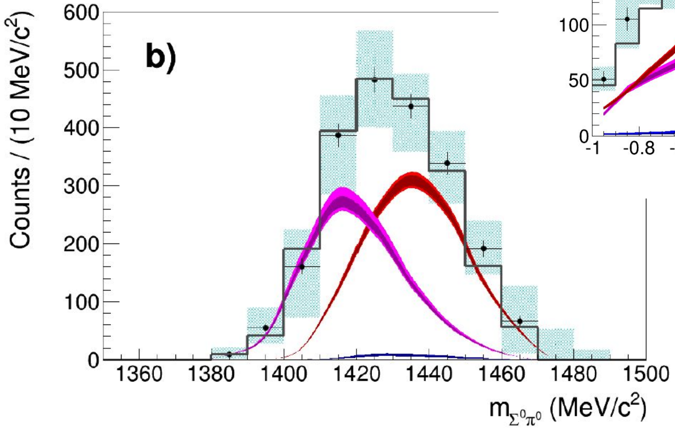

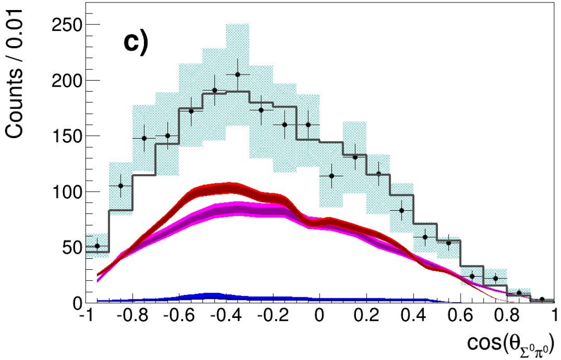

FIG. 3. From top to bottom the figure shows the result of the simultaneous fit of $p_{\Sigma^0\pi^0}$, $m_{\Sigma^0\pi^0}$ and $cos\theta_{\Sigma^0\pi^0}$. The experimental data and the corresponding statistical errors are represented by black crosses, the systematic errors are light blue boxes. The contributions of the various physical processes are shown as colored histograms, according to the color code shown in the caption. The light and dark bands correspond to systematic and statistical errors, respectively. The gray distribution reproduces the global fit function.

preliminary

Simultaneous fit and cross sections $(\Lambda\,\pi^0)$

+ the same processes initiated by primary $\Sigma^0\,\pi^0$ and followed by $\Sigma^0 \to \Lambda\gamma$

physical processes:

1. $K^- H \;\to\; (\Sigma^0/\Lambda)\,\pi^0\; if$ (red),
2. $K^- H \;\to\; (\Sigma^0/\Lambda)\,\pi^0\; ar$ (blue),
3. $K^- + {}^4He/{}^{12}C \;\to\; \Sigma^0/\Lambda + \pi^0 + {}^3H/{}^{11}B$ (magenta).

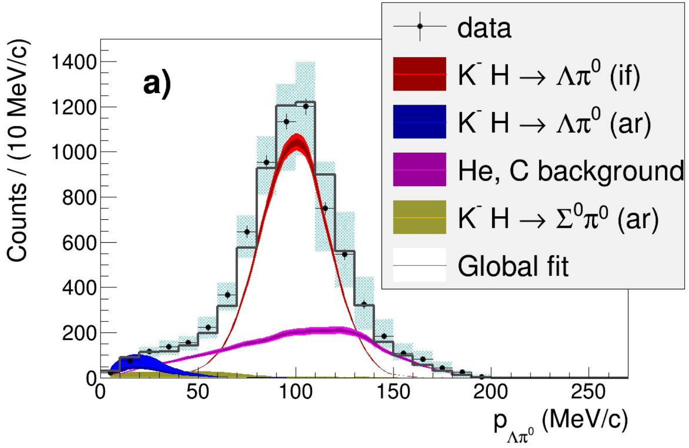

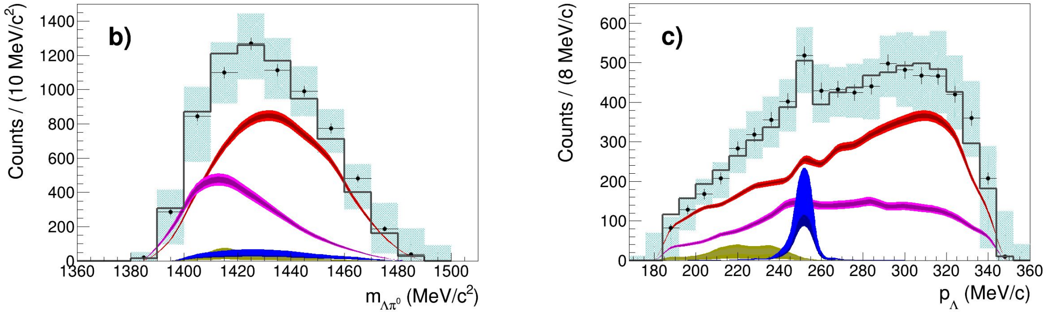

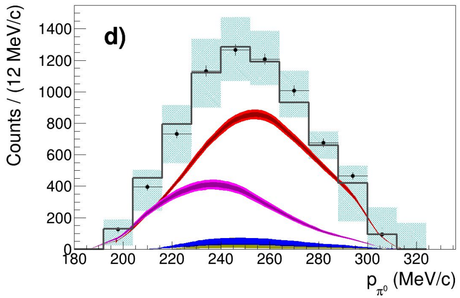

FIG. 4. From top to bottom the figure shows the result of the simultaneous fit of $p_{\Lambda\pi^0}$, $m_{\Lambda\pi^0}$, p_Λ and p_{π^0}. The experimental data and the corresponding statistical errors are represented by black crosses, the systematic errors are light blue boxes. The contributions of the various physical processes are shown as colored histograms, according to the color code shown in the caption. The light and dark bands correspond to systematic and statistical errors, respectively. The gray distribution reproduces the global fit function.

preliminary

Cross sections results

$\Sigma^0-\pi^0$ CHANNEL	$\frac{\chi^2}{(dof-np)}=\frac{92}{54}=1.71$	
process	fit par. value	$\sigma_{stat.}$
$K^-H\to\Sigma^0\pi^0\,(if)$	0.511	$\pm$ 0.018
$K^-H\to\Sigma^0\pi^0\,(ar)$	0.017	$\pm$ 0.005
$K^-+^4He/^{12}C\to\Sigma^0\pi^0$		
+ residual (ar/if)	0.463	$\pm$ 0.018
$\Lambda-\pi^0$ CHANNEL	$\frac{\chi^2}{(dof-np)}=\frac{165}{57}=2.95$	
process	fit par. value	$\sigma_{stat.}$
$K^-H\to\Lambda\pi^0\,(if)$	0.659	$\pm$ 0.011
$K^-H\to\Lambda\pi^0\,(ar)$	0.021	$\pm$ 0.003
$K^-+^4He/^{12}C\to\Lambda\pi^0$		
+ residual (ar/if)	0.298	$\pm$ 0.012
$K^-H\to\Sigma^0\pi^0$		
$\to\Lambda\gamma\pi^0\,(ar)$	0.018	$\pm$ 0.006

TABLE I. The table summarizes the results obtained from the fits of the $\Sigma^0\pi^0$ and $\Lambda\pi^0$ samples. The values of the reduced chi-squares and of the fit parameters are summarized.

cross section at p_{K^-} = 98 ± 10 MeV/c :

- $\sigma_{K^-p\to\Sigma^0\pi^0}=42.8\pm1.5(stat.)^{+2.4}_{-2.0}(syst.)$ mb
- $\sigma_{K^-p\to\Lambda\pi^0}=31.0\pm0.5(stat.)^{+1.2}_{-1.2}(syst.)$ mb ,

th. calculation
Y. Ikeda, T. Hyodo, W. Weise,
Nucl. Phys. A 881 (2012) 98

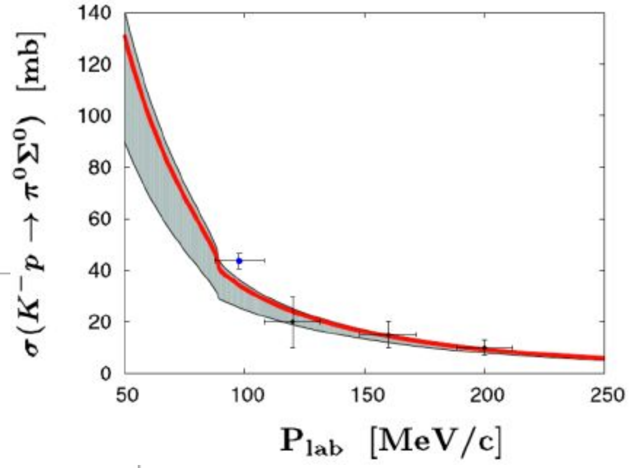

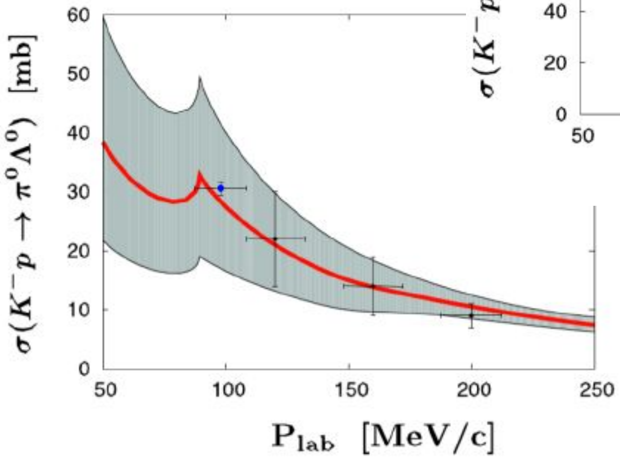

preliminary

First simultaneous $K^- p \rightarrow (\Sigma^0/\Lambda)\,\pi^0$ cross sections measurement below 100 MeV/c

Kristian Piscicchia[a,b], Magdalena Skurzok[c], Michael Cargnelli[d,b], Raffaele Del Grande[e,b], Laura Fabbietti[f,e], Johann Marton[d,b], Pawel Moskal[c], Alessandro Scordo[b], Àngels Ramos[g], Diana Laura Sirghi[b,h], Oton Vazquez Doce[b], Johann Zmeskal[d,b], Sławomir Wycech[g] and Catalina Curceanu[b,h]

[a] *Centro Ricerche Enrico Fermi - Museo Storico della Fisica e Centro Studi e Ricerche "Enrico Fermi", Roma, Italy, EU*
[b] *Laboratori Nazionali di Frascati INFN, Frascati (Rome), Italy, EU*
[c] *Institute of Physics, Jagiellonian University, Cracow, Poland, EU*
mskurzok@gmail.com
[d] *Stefan-Meyer-Institute for subatomic physics, Austrian Academy of Science, Austria, EU*
[e] *Physik Department E62, Technische Universität München, Garching, Germany, EU*
[f] *Excellence Cluster "Origin and Structure of the Universe", Garching, Germany, EU*
[g] *Facultat de Física, Universitat de Barcelona, Barcelona, Spain, EU*
[h] *IFIN-HH, Institutul National pentru Fizica si Inginerie Nucleara Horia Hulubei, Romania, EU*
[g] *National Centre for Nuclear Research, Warsaw, Poland, EU*

The first simultaneous measurements of the $K^- p \rightarrow \Sigma^0\,\pi^0$ and $K^- p \rightarrow \Lambda\,\pi^0$ cross sections were performed, below 100 MeV/c kaon momentum. The kaon beam delivered by the DAΦNE collider was exploited to detect K^- absorptions on Hydrogen atoms, populating the gas mixture of the KLOE drift chamber. The precision of the measurements ($\sigma_{K^-p\rightarrow\Sigma^0\pi^0} = 42.8 \pm 1.5(stat.)^{+2.4}_{-2.0}(syst.)$ mb and $\sigma_{K^-p\rightarrow\Lambda\pi^0} = 31.0 \pm 0.5(stat.)^{+1.2}_{-1.2}(syst.)$ mb) is the highest yet obtained in the low kaon momentum regime.

Ongoing - $\Sigma^0\ \pi^0$ invariant mass studies to extract the $\Lambda(1405)$ shape

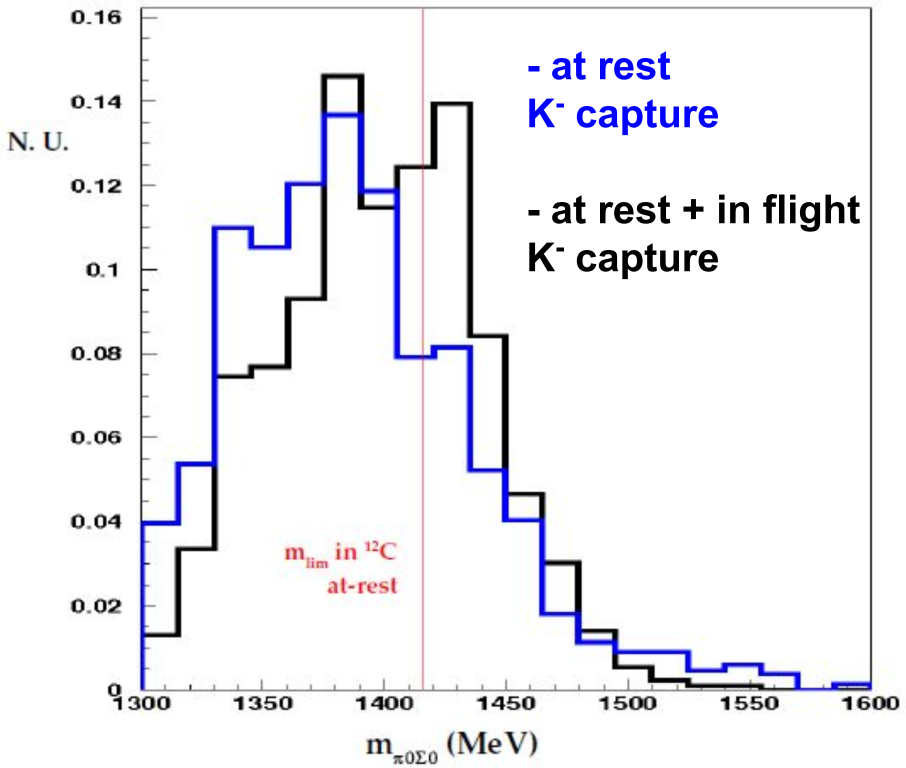

Same analysis for the I = 0 counterpart.

measured channel:

$K^- p \rightarrow \Sigma^0\ \pi^0$

(bound proton in ^{12}C)

for the extraction of the $\Lambda(1405)$ shape

$p_{\pi 0}$ resolution: $\sigma_p \approx 12$ MeV/c

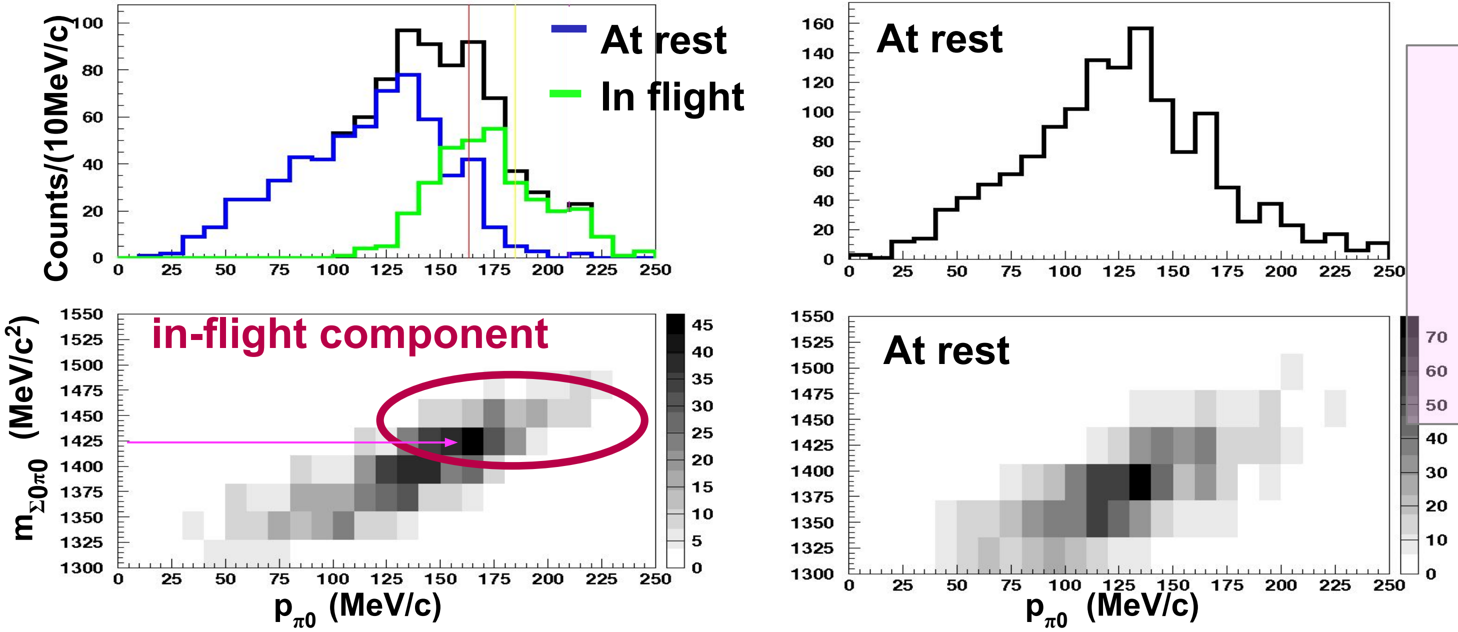

IN-FLIGHT

K- 12C

opens a window

between 1416 MeV

and K-Nth

difficulty: epoxy resin, contained in the carbon fibre target, contains H

H atoms in the molecules mainly contribute to **K- H absorption in-flight**, resulting in a **non-resonant background in the Σ^0 π^0 spectra**

$K^- p \rightarrow \Sigma^+ \pi^-$ (bound proton in ^{12}C)

p_π resolution about 1MeV → K- capture at-rest/in-flight/on H can be distinguished

K.P. et al. Acta Phys. Pol. B 48, 1875 (2017)

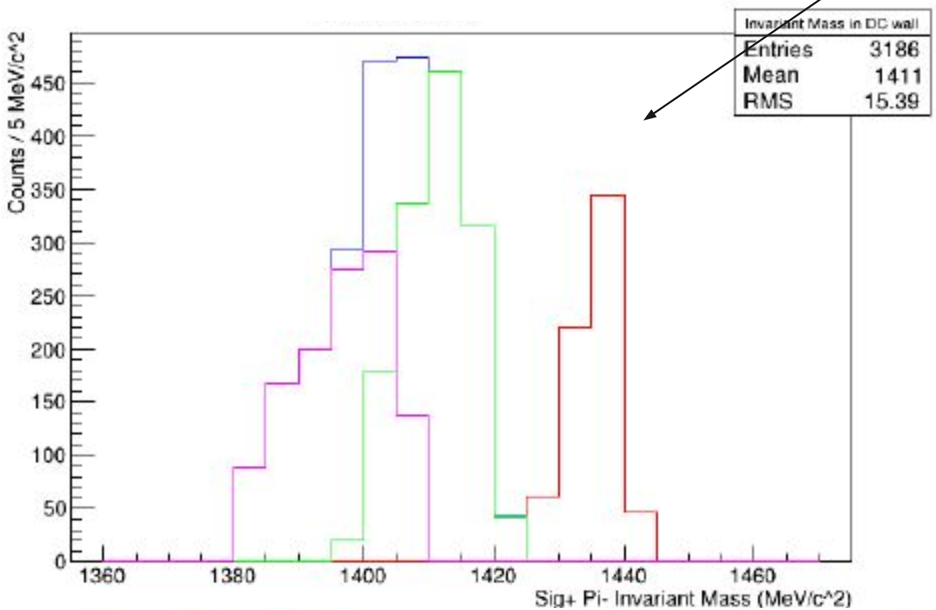

Figure 3: *(Colour online.) $m_{\Sigma\pi}$ invariant mass distributions in-flight (green) and at-rest (violet) in ^{12}C. Blue histogram represents the sum of green and violet histograms. The red distribution refers to K^- absorptions on Hydrogen*

but, neglecting the small I = 2 component

$$\frac{d\sigma(\pi^+\Sigma^-)}{dM_I} \propto \frac{1}{3}|T^{(0)}|^2 + \frac{1}{2}|T^{(1)}|^2 + \frac{2}{\sqrt{6}}\mathrm{Re}\,(T^{(0)}T^{(1)*}),$$

$$\frac{d\sigma(\pi^-\Sigma^+)}{dM_I} \propto \frac{1}{3}|T^{(0)}|^2 + \frac{1}{2}|T^{(1)}|^2 - \frac{2}{\sqrt{6}}\mathrm{Re}\,(T^{(0)}T^{(1)*}),$$

$$\frac{d\sigma(\pi^0\Sigma^0)}{dM_I} \propto \frac{1}{3}|T^{(0)}|^2,$$

K^- multi-nucleon absorptions

In order to fit the kaonic atoms data a K^- multi-nucleon absorption term is necessary in the K^--nuclei optical potential:

$$V_{K^-}(\rho) = V_{K^-}^{(1)}(\rho) + V_{K^-}^{(2)}(\rho)$$

→ **phen. multi-nucleon term**

[E. Friedman, A. Gal, Nucl. Phys. A 959, 66 (2017)]
[Hrtánková, J. & Mareš, J. Phys. Rev. C96, 015205 (2017)]

single nucleon term from chiral models

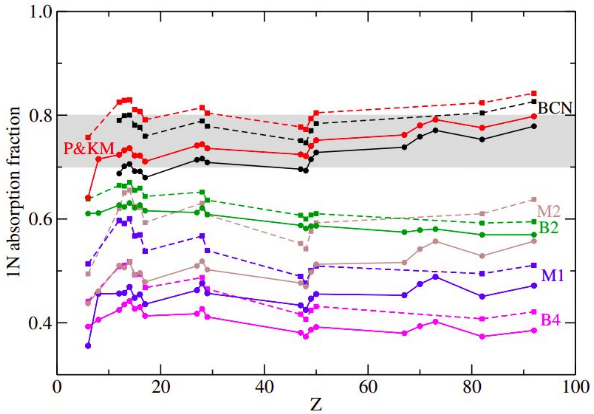

- **Single nucleon absorption (1NA):** K^- "N" → Y π
- **Two nucleon absorption (2NA):** K^- "NN" → Y N
- **Three nucleon absorption (3NA):** K^- "NNN" → Y (NN)
- **Four nucleon absorption (4NA):** K^- "NNNN" → Y (NNN)

→ multi-N processes

bound nucleons = "N", "NN", "NNN", "NNNN"
bound or unbound nucleons = (NN), (NNN)
Y = Λ, Σ

Λp analysis: $K^- + {}^{12}C \rightarrow \Lambda + p + R$

Simultaneous fit of:

- Λp invariant mass;
- angular correlation;
- proton momentum;
- Λ momentum.

Total reduced χ^2: $\chi^2/dof = 0.94$

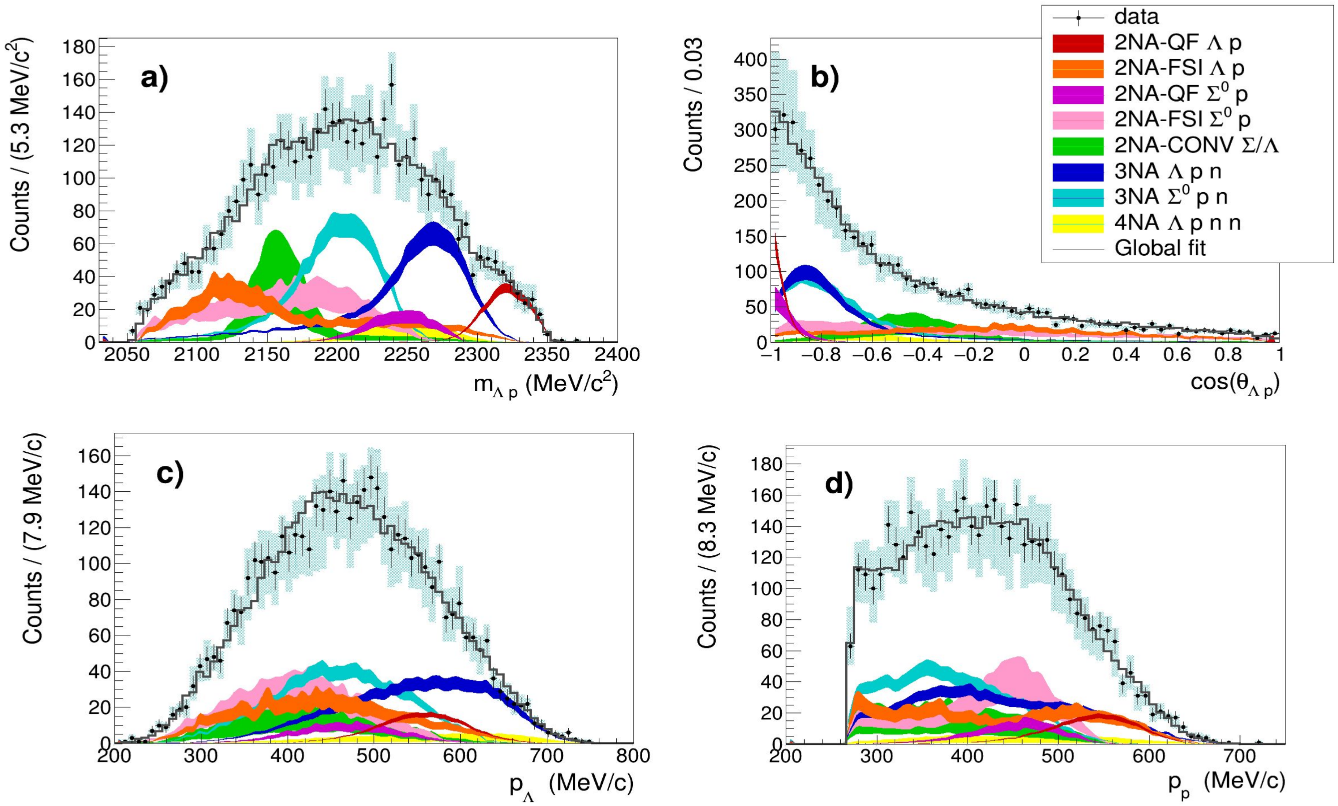

[R. Del Grande, K. P., O. Vazquez Doce et al., Eur.Phys.J. C79 (2019) no.3, 190]
[R. Del Grande, K. P., S. Wycech, Acta Phys. Pol. B 48 (2017) 1881]
[O. Vazquez Doce, L. Fabbietti et al., Phys.Lett. B 758, 134-139 (2016)]

Λp analysis: K⁻ multi-nucleon absorption BRs and σ

[R. Del Grande, K. P., O. Vazquez Doce et al., Eur.Phys.J. C79 (2019) no.3, 190]

Process	Branching Ratio (%)	σ (mb)	@	p_K (MeV/c)
2NA-QF Λp	0.25 ± 0.02 (stat.) $^{+0.01}_{-0.02}$(syst.)	2.8 ± 0.3 (stat.) $^{+0.1}_{-0.2}$ (syst.)	@	128 ± 29
2NA-FSI Λp	6.2 ± 1.4(stat.) $^{+0.5}_{-0.6}$(syst.)	69 ± 15 (stat.) $\pm$ 6 (syst.)	@	128 ± 29
2NA-QF Σ^0p	0.35 ± 0.09(stat.) $^{+0.13}_{-0.06}$(syst.)	3.9 ± 1.0 (stat.) $^{+1.4}_{-0.7}$ (syst.)	@	128 ± 29
2NA-FSI Σ^0p	7.2 ± 2.2(stat.) $^{+4.2}_{-5.4}$(syst.)	80 ± 25 (stat.) $^{+46}_{-60}$ (syst.)	@	128 ± 29
2NA-CONV Σ/Λ	2.1 ± 1.2(stat.) $^{+0.9}_{-0.5}$(syst.)	-		
3NA Λpn	1.4 ± 0.2(stat.) $^{+0.1}_{-0.2}$(syst.)	15 ± 2 (stat.) $\pm$ 2 (syst.)	@	117 ± 23
3NA Σ^0pn	3.7 ± 0.4(stat.) $^{+0.2}_{-0.4}$(syst.)	41 ± 4 (stat.) $^{+2}_{-5}$ (syst.)	@	117 ± 23
4NA Λpnn	0.13 ± 0.09(stat.) $^{+0.08}_{-0.07}$(syst.)	-		
Global $\Lambda(\Sigma^0)$p	21 ± 3(stat.) $^{+5}_{-6}$(syst.)	-		

The ratio between the branching ratios of the 2NA-QF in the Λp channel and in the Σ^0p is measured to be:

$$\mathcal{R} = \frac{BR(K^- pp \rightarrow \Lambda p)}{BR(K^- pp \rightarrow \Sigma^0 p)} = 0.7 \pm 0.2(stat.)^{+0.2}_{-0.3}(syst.)$$

and the ratio between the corresponding phase spaces is $\mathcal{R}' \simeq 1.22$.

Information on the in-medium dynamics

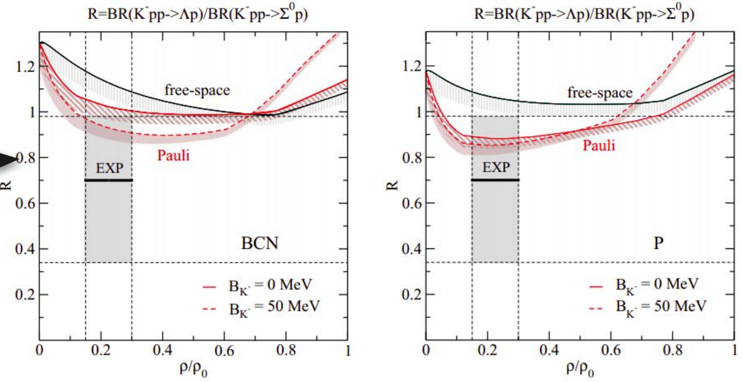

[J. Hrtánková and A. Ramos. Phys. Rev. C, 101(3):035204, 2020]

Total BR of the K^- 2NA process in ^{12}C

the only missing components are:

- BR($\Sigma^- n$) = (0.12 ± 0.01(syst.))%
- BR(QF-Λn + QF-$\Sigma^0 n$) = $(0.76 \pm 0.09(\text{stat.})\ ^{+0.13}_{-0.06}\ (\text{syst.}))\%$
- BR(FSI-Λn + FSI-$\Sigma^0 n$) = $(1.62 \pm 0.04(\text{stat.})\ ^{+0.22}_{-0.21}\ (\text{syst.}))\%$
- BR(no conv Σ^+ and Σ^-) = (3.04 ± 0.03(stat.) ± 0.92(syst.))%

→ $(5.5 \pm 0.1(\text{stat.})\ ^{+1.0}_{-0.9}\ (\text{syst.}))\%$

[R. Del Grande, K. P., et al., 2020 Phys. Scr.95 084012]
[R. Del Grande, K. P., et al., *Few Body Syst.* 62 (2021) 1, 7]

Including the missing components the total BR of the K^-2NA is:

$$\mathrm{BR}(\mathrm{K}^-2\mathrm{NA} \rightarrow \mathrm{YN}) = (21.6 \pm 2.9(\mathrm{stat.})^{+4.4}_{-5.6}(\mathrm{syst.}))\%$$

to be compared with [J. Hrtánková and A. Ramos. Phys. Rev. C, 101(3):035204, 2020]

Λp analysis: K⁻ pp bound state

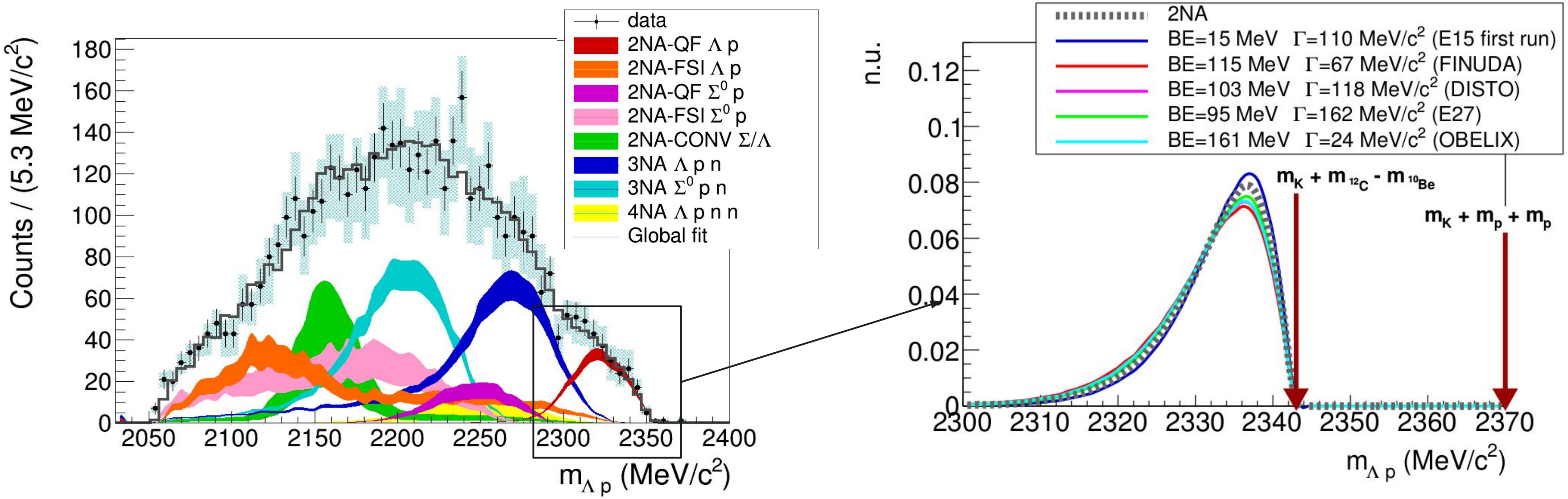

K^-pp bound state contribution **completely overlaps** with the K^-2NA

Λp analysis: K^- pp bound state

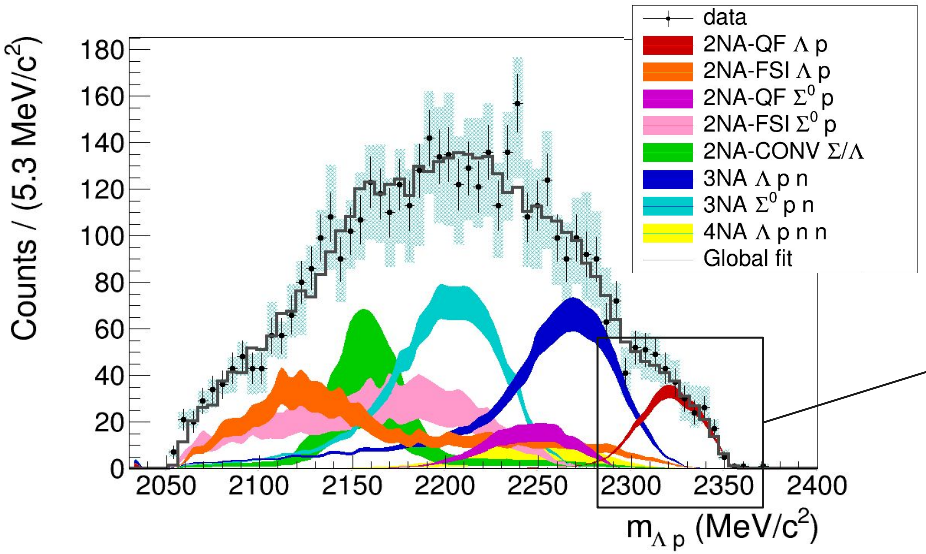

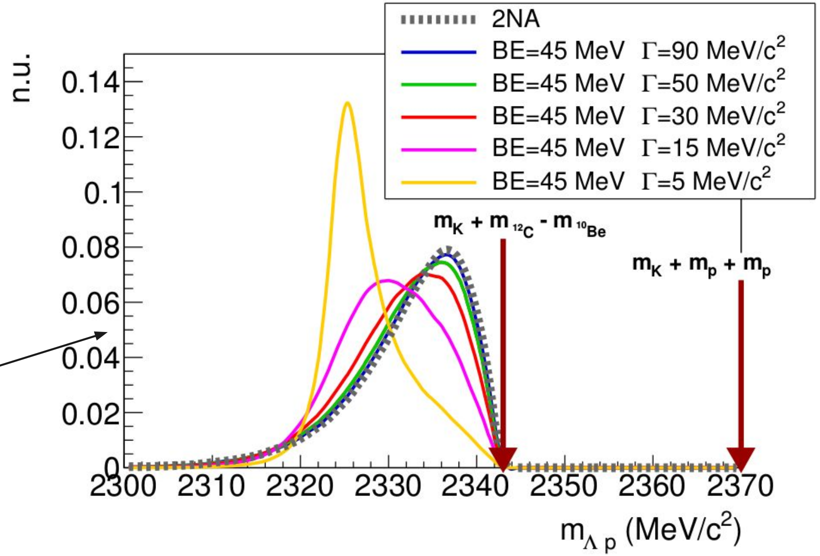

K^-pp bound state contribution **completely overlaps** with the K^-2NA

Λp analysis: K⁻ pp bound state search

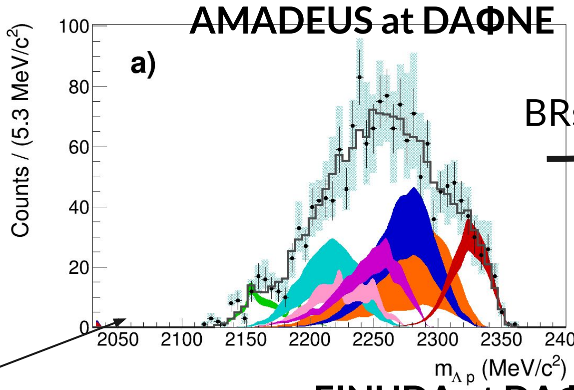

BRs evaluation

Process	Branching Ratio (%)
2NA-QF Λp	$0.20 \pm 0.04(\text{stat.}) \pm 0.02(\text{syst.})$
2NA-FSI Λp	$3.8 \pm 2.3(\text{stat.}) \pm 1.1(\text{syst.})$
2NA-QF Σ^0p	$0.54 \pm 0.20(\text{stat.})\ ^{+0.20}_{-0.16}(\text{syst.})$
2NA-FSI Σ^0p	$5.4 \pm 1.5(\text{stat.})\ ^{+1.0}_{-2.7}(\text{syst.})$
2NA-CONV Σ/Λ	$22 \pm 4(\text{stat.})\ ^{+1}_{-12}(\text{syst.})$
3NA Λpn	$1.1 \pm 0.3(\text{stat.}) \pm 0.2(\text{syst.})$
3NA Σ^0pn	$1.9 \pm 0.7(\text{stat.})\ ^{+0.8}_{-0.4}(\text{syst.})$

only back-to-back Λp pairs ($\cos\theta_{\Lambda p} < -0.8$)

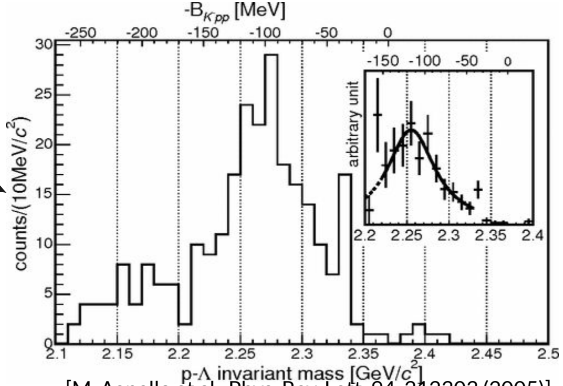

[M. Agnello et al., Phys. Rev. Lett. 94, 212303 (2005)]

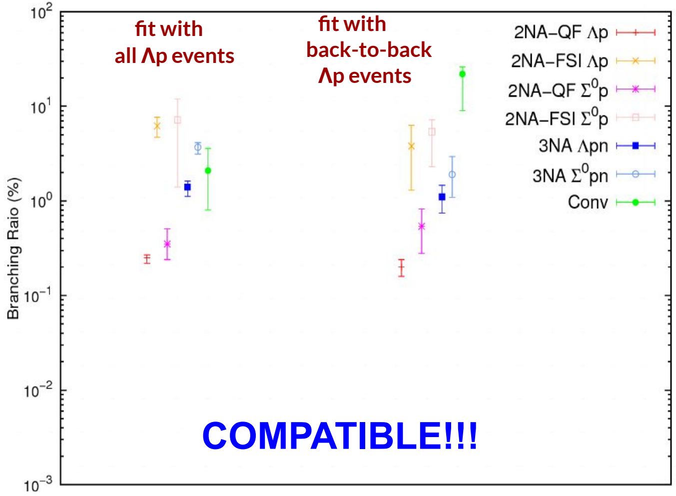

In agreement with

V.K. Magas, E. Oset, A. Ramos, H. Toki,. Phys. Rev. C 74, 025206 (2006)
V.K. Magas, E. Oset, A. Ramos,. Phys. Rev. C 77, 065210 (2008)

Λt analysis: Cross section and BR for 4NA

GOLDEN CHANNEL to extrapolate the K^- 4NA

K^- + "ppnn" → Λ + t

Previous data:

- in ^{4}**He:** bubble chamber experiment
/M. Roosen, J. H. Wickens, Il Nuovo Cimento 66, 101 (1981)/
only **3 events** compatibile with Λt kinematics found

BR($K^{-4}He$ → Λt) = (3 ± 2) × 10^{-4} /K_{stop} → global, no 4NA

- in **solid targets:** ^{6,7}**Li,** ^{9}**Be** (FINUDA)
/Phys. Lett. B, 229 (2008)/
40 events, only **back-to-back data**

Λt emission yield → 10^{-3} – 10^{-4} / K^-_{stop}

→ global, no 4NA

PRELIMINARY

AMADEUS analysis

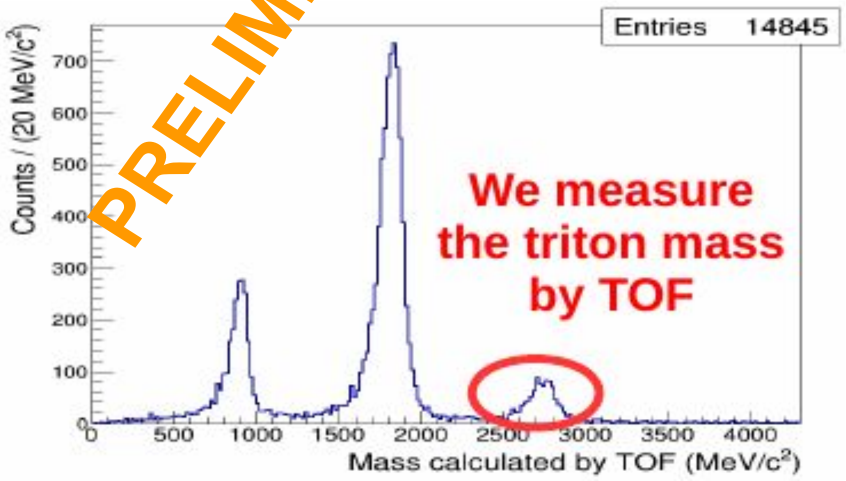

MC simulations: efficiency & resolution

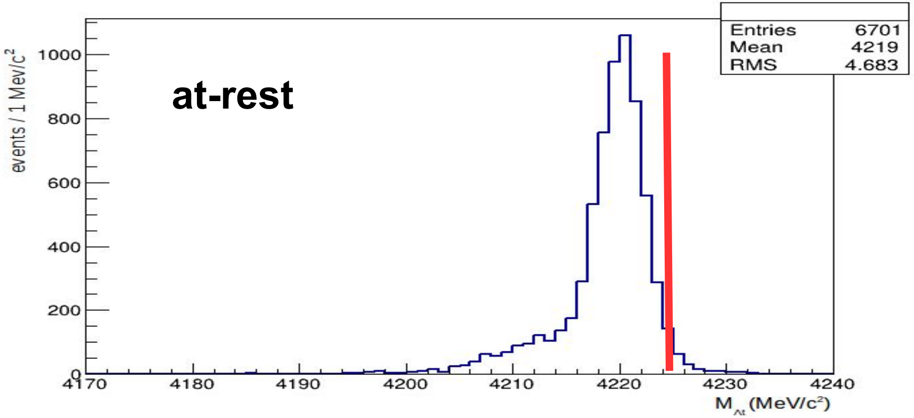

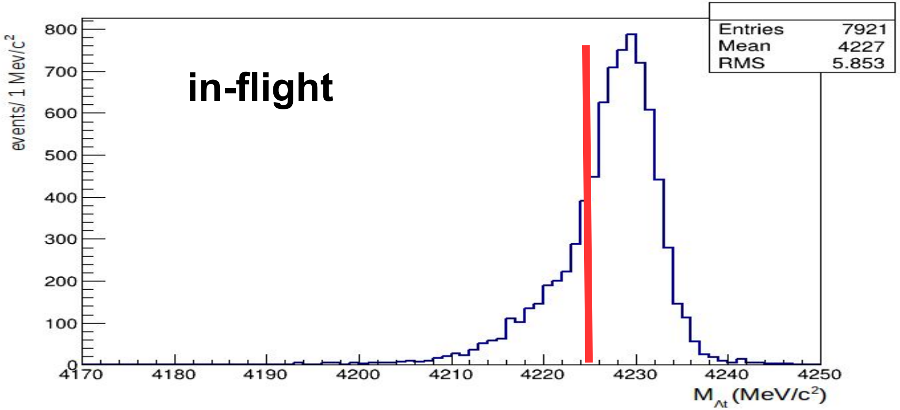

mass threshold at-rest

$M_{\Lambda t}$ invariant mass resolution = 2.2 MeV/c^2

overall <u>detection + reconstruction efficiency</u> for 4NA direct Λt production :

$$\epsilon_{4\mathrm{NA},ar,\Lambda t} = 0.0493 \pm 0.0006 \quad ; \quad \epsilon_{4\mathrm{NA},if,\Lambda t} = 0.0578 \pm 0.0006,$$

at-rest **in-flight**

Cross section and BR for 4NA in $K^{-}\,{}^{4}He \rightarrow \Lambda t$ process

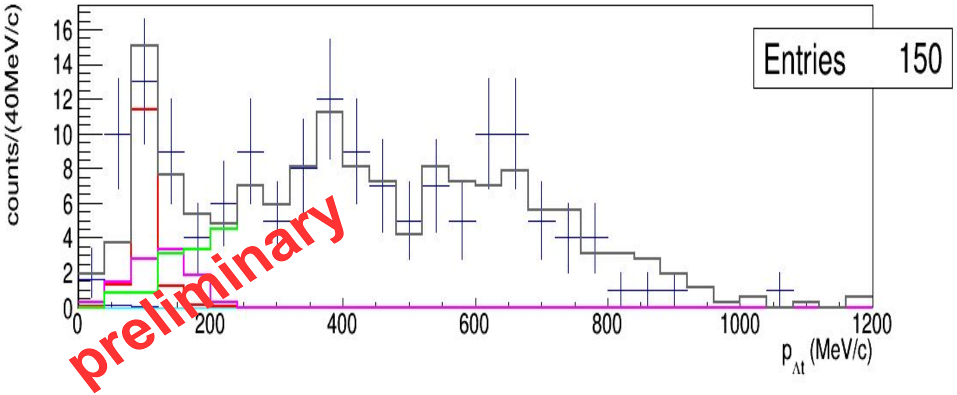

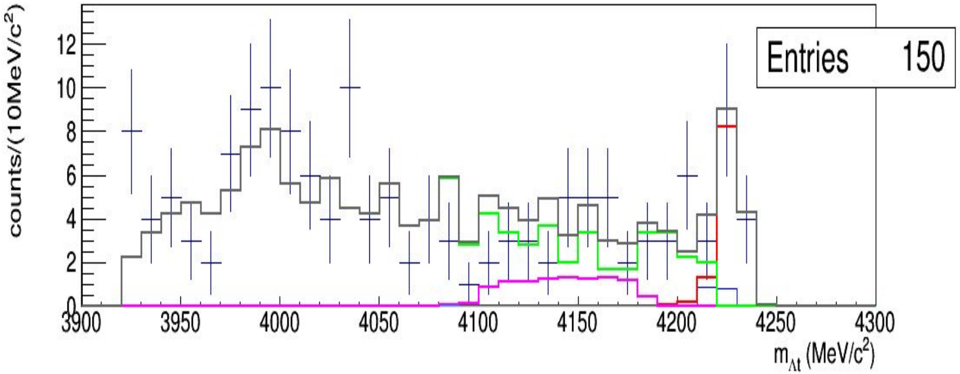

BR$(K^{-4}He(4NA) \rightarrow \Lambda t)$ **< 2.0 × 10^{-4} /K$_{stop}$ (95% c. l.)**

σ(100 ± **19** MeV/c) $(K^{-4}He(4NA) \rightarrow \Lambda t)$ =

= (0.81 ± 0.21 (stat) $^{+0.03}_{-0.04}$ (syst)) mb

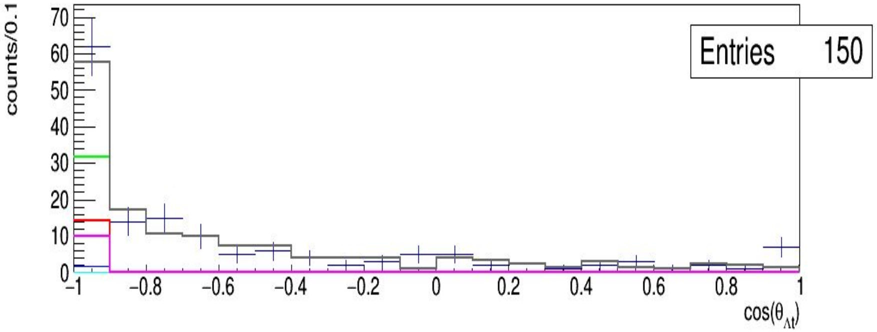

Cross section and BR for 4NA in $K^{-}\,{}^{12}C \to \Lambda/\Sigma^0\, t$ processes

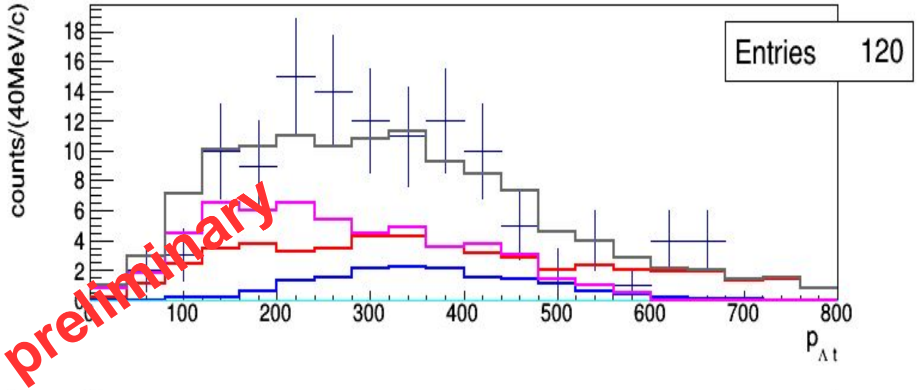

BR($K^{-12}C$(4NA) → $\Lambda t\, {}^8Be$) = **1.5 ± 0.5 × 10^{-4} (stat) /K_{stop}**

σ($K^{-12}C$ (4NA) →$\Lambda t\, {}^8Be$) = **0.58 ± 0.11 (stat) mb**

σ($K^{-12}C$ (4NA) →$\Sigma^0 t\, {}^8Be$) = **1.88 ± 0.35 (stat) mb**

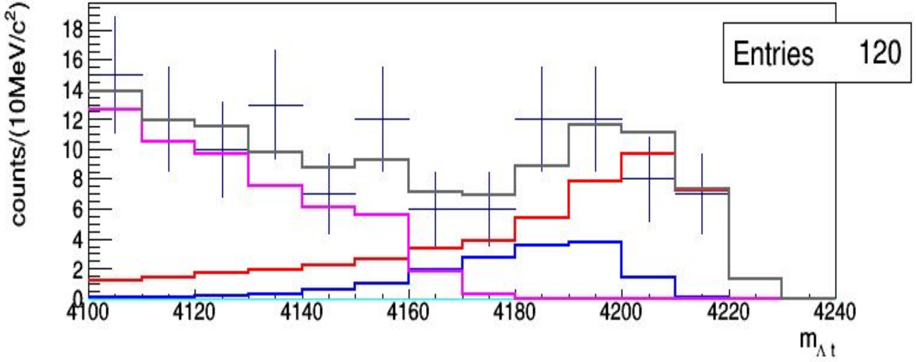

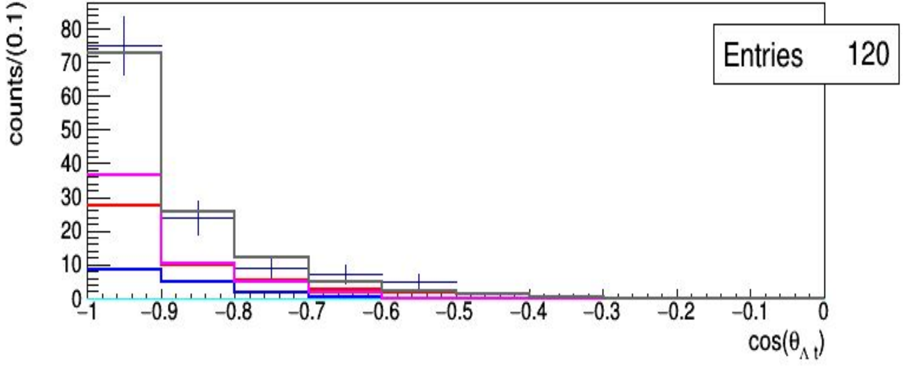

Future perspectives

$(K^- \ ppn) + n \ \rightarrow \ \Sigma^0 \, d + n$

3NA in ^{4}He

for the investigation of the

Σ^0-N & Σ^0-(NN) interaction

Involved reactions:

3NA - $(K^- ppn) + n \rightarrow \Sigma^0 d + n$

- The Σ^0 identification (with respect to Λ) we don't deal with internal conversion background. Moreover Σ^0-N scattering data is demanded.

- ^4He target $\rightarrow$ no nuclear fragmentation can follow the 3NA primary process.

+

3NA can be followed by two possible elastic FSI

1) n d $\rightarrow$ n d we may take advantage of the well known σNN data

2) Σ^0 n/d $\rightarrow$ Σ^0 n/d from which to extract information on Σ^0-N , Σ^0-(NN) interaction.

Involved reactions - signal:

3NA - $(K^- ppn) + n \rightarrow \Sigma^0 d + n$

- **Preliminary comparison of 3NA simulations with $K^- \, ^{12}C \rightarrow \Sigma^0 d + R$ data.**

- **We assume the negative kaon to be absorbed on one of the three α particles**

- **We show that the most energetic part of the $m_{\Sigma 0d}$ invariant mass spectrum is correlated to high $p_{\Sigma 0}$ and p_d momenta, this corresponds to the 3NA - $(K^- ppn)$ process.**

The Σ^0 d statistics from K- captures in the gas filling the KLOE DC is poor. Moreover K- in ^{12}C (from isobutane) are not distinguishable from K- captures on ^4He.

Dedicated measurement with pure ^4He target (^3He target also helpful for comparison) is mandatory for this purpose.

3NA

$(K^- ppn) + n \rightarrow \Sigma^0 d + n$

without FSI

Corresponds to the highest part of the invariant mass spectrum

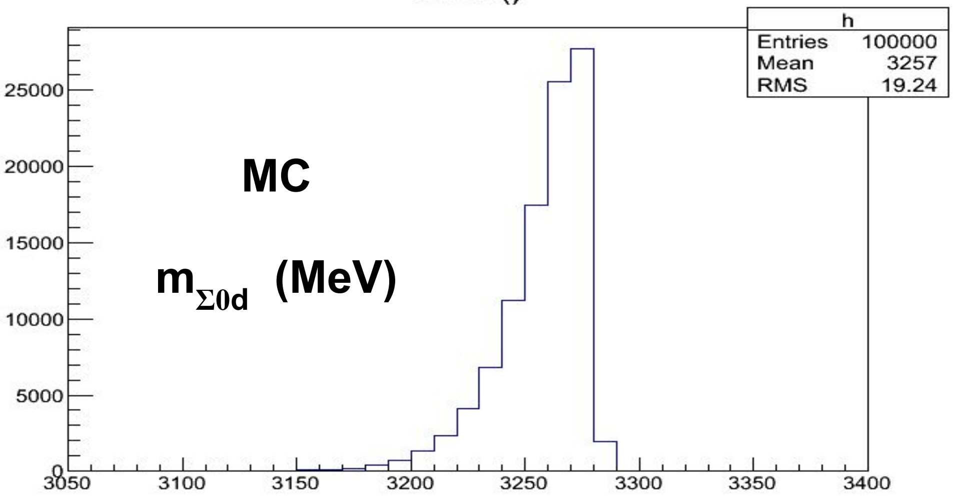

the blue region is populated by free 3NA,

at slightly lower energy is the 3NA followed by 2B & 3B FSI.

Our aim is to measure the relative contributions of the two processes.

At lower energies 2NA is involved and complex FSI processes with fragmentation of the residual ^8Be (not present in ^4He target).

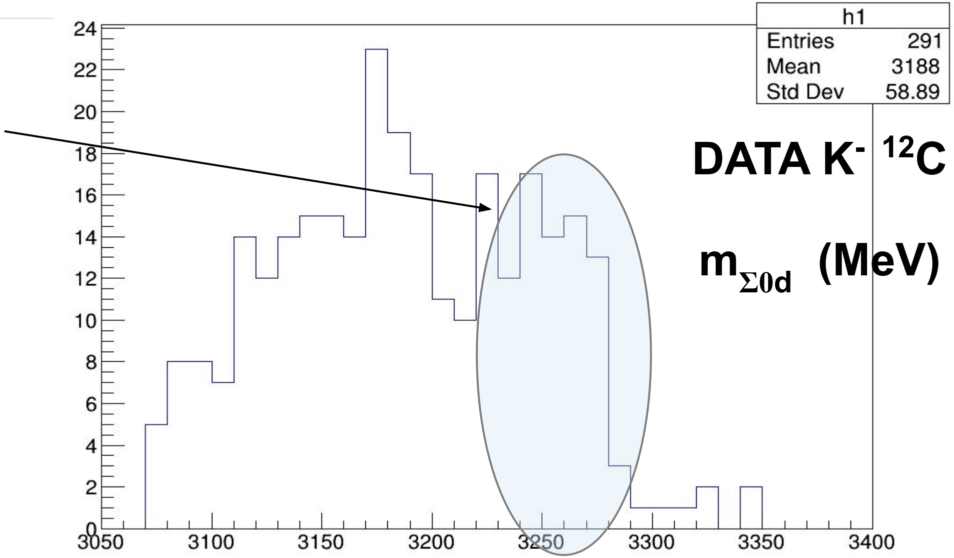

<u>3NA</u>

(K⁻ ppn) + n → Σ⁰ d + n

without FSI

Corresponds to the highest part of the Σ⁰ momentum spectrum.

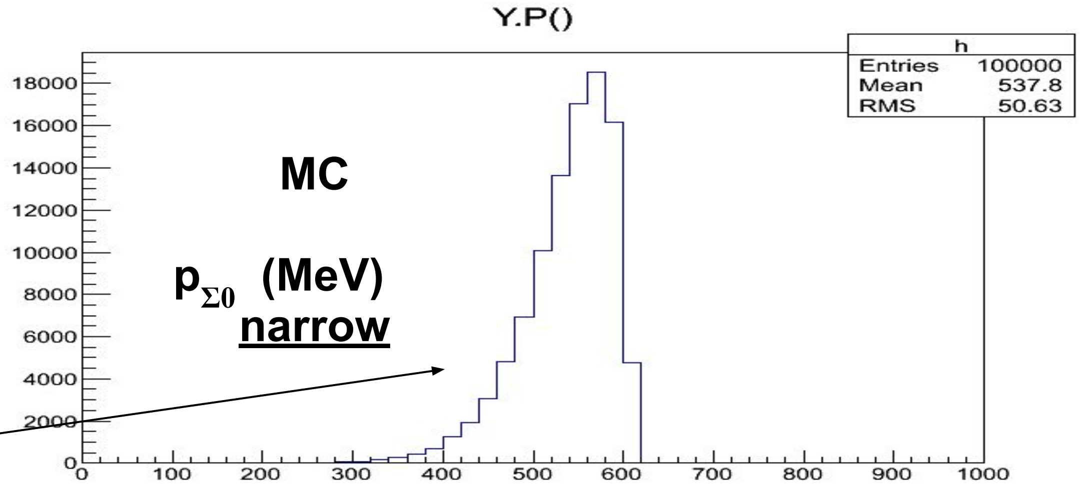

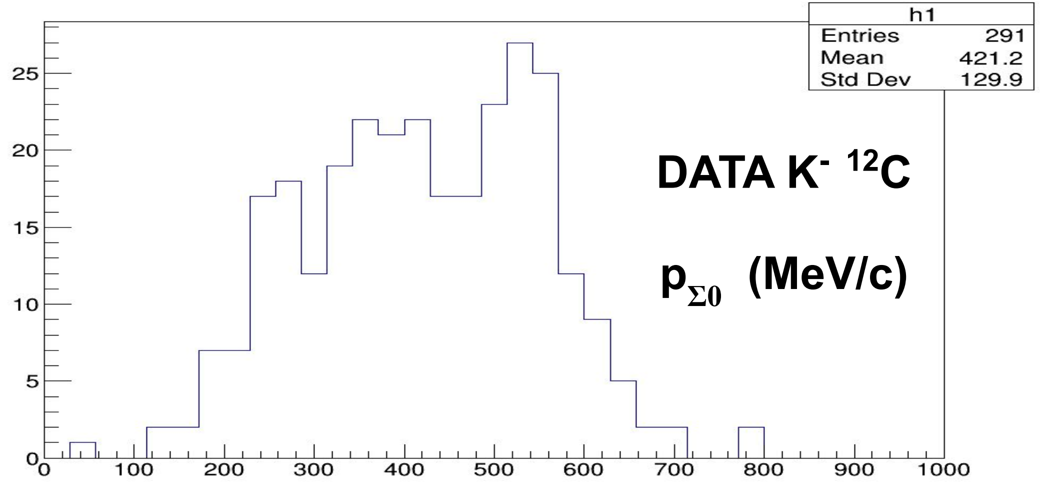

The narrow Σ^0 momentum distribution yields Σ^0-N and Σ^0-NN cross section at 550 ± 50 MeV/c.

Accurate model of the:

$(K^- ppn) + n \rightarrow \Sigma^0 d + n$

3NA in ^4He

+

$\Sigma^0 d/n \rightarrow \Sigma^0 d/n$ **FSI**

is needed to extract the corresponding cross sections from the measured shapes.

Summary

K⁻n amplitude below threshold

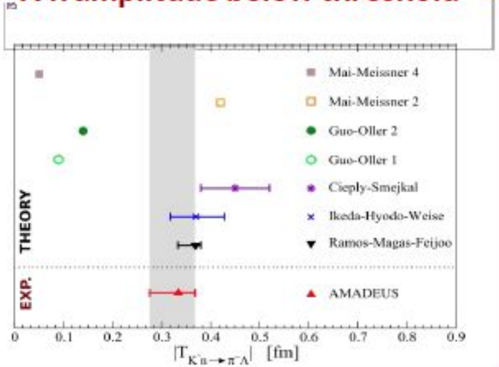

Λ p channel: 2NA, 3NA and 4NA BRs and σ

Process	Branching Ratio (%)	σ (mb)	@	p_K (MeV/c)
2NA-QF Λp	0.25 ± 0.02 (stat.) $^{+0.01}_{-0.02}$(syst.)	2.8 ± 0.3 (stat.) $^{+0.1}_{-0.2}$ (syst.)	@	128 ± 29
2NA-FSI Λp	6.2 ± 1.4(stat.) $^{+0.5}_{-0.6}$(syst.)	69 ± 15 (stat.) ± 6 (syst.)	@	128 ± 29
2NA-QF Σ^0p	0.35 ± 0.09(stat.) $^{+0.13}_{-0.06}$(syst.)	3.9 ± 1.0 (stat.) $^{+1.4}_{-0.7}$ (syst.)	@	128 ± 29
2NA-FSI Σ^0p	7.2 ± 2.2(stat.) $^{+4.2}_{-5.4}$(syst.)	80 ± 25 (stat.) $^{+46}_{-60}$ (syst.)	@	128 ± 29
2NA-CONV Σ/Λ	2.1 ± 1.2(stat.) $^{+0.9}_{-0.5}$(syst.)	-		
3NA Λpn	1.4 ± 0.2(stat.) $^{+0.1}_{-0.2}$(syst.)	15 ± 2 (stat.) ± 2 (syst.)	@	117 ± 23
3NA Σ^0pn	3.7 ± 0.4(stat.) $^{+0.2}_{-0.4}$(syst.)	41 ± 4 (stat.) $^{+2}_{-5}$ (syst.)	@	117 ± 23
4NA Λpnn	0.13 ± 0.09(stat.) $^{+0.08}_{-0.07}$(syst.)	-		
Global $\Lambda(\Sigma^0)$p	21 ± 3(stat.) $^{+5}_{-6}$(syst.)	-		

The ratio between the branching ratios of the 2NA-QF in the Λp channel and in the Σ^0p is measured to be:

$$\mathcal{R} = \frac{BR(K^-pp \to \Lambda p)}{BR(K^-pp \to \Sigma^0 p)} = 0.7 \pm 0.2(stat.)^{+0.2}_{-0.3}(syst.)$$

$$\mathrm{BR}(K^-2NA \to YN) = (21.6 \pm 2.9(\mathrm{stat.})^{+4.4}_{-5.6}(\mathrm{syst.}))\%$$

Preliminary K- p -> $(\Sigma^0/\Lambda)\ \pi^0$

cross section at p_{K^-} = 98 ± 10 MeV/c :

- $\sigma_{K^-p\to\Sigma^0\pi^0} = 42.8 \pm 1.5(stat.)^{+2.4}_{-2.0}(syst.)$ mb
- $\sigma_{K^-p\to\Lambda\pi^0} = 31.0 \pm 0.5(stat.)^{+1.2}_{-1.2}(syst.)$ mb ,

Λ t channel: 4NA BRs and σ

BR(K^{-4}He(4NA) → Λt) < 2.0 × 10^{-4} /K_{stop} (95% c. l.)
σ(100 ± 19 MeV/c) (K^{-4}He(4NA) → Λt) =
= (0.81 ± 0.21 (stat) $^{+0.03}_{-0.04}$ (syst)) mb

BR(K^{-12}C(4NA) → Λt ^{8}Be) = 1.5 ± 0.5 × 10^{-4} (stat) /K_{stop}
σ(K^{-12}C (4NA) → Λt ^{8}Be) = 0.58 ± 0.11 (stat) mb
σ(K^{-12}C (4NA) → Σ^0t ^{8}Be) = 1.88 ± 0.35 (stat) mb

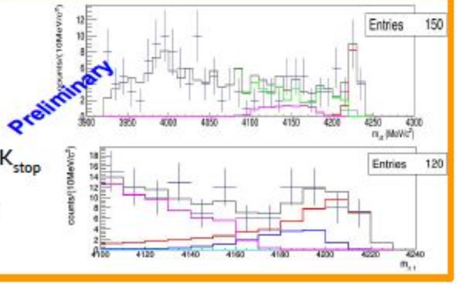

Thank You

$K^-(s=0)$ $^4He(s=0)$ $n(s=1/2)$ $\Sigma^{*-}(s=3/2) \rightarrow$ resonance p-wave only

atomic s-state capture:

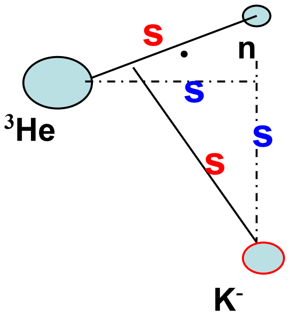

(K⁻ n) s-state interaction

Σ^{*-} not allowed

NON-RES only

• +

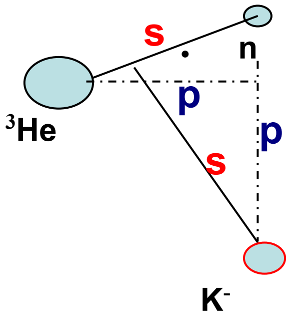

consequence of 3-body effect

(K⁻ n) p-state interaction

Σ^{*-} allowed

- $(K^- \, ^4He \rightarrow \Lambda\pi^- \, ^3He)$ absorptions from (n s) - atomic states are assumed →

^{4}He bubble chamber data (Fetkovich, Riley interpreted by Uretsky, Wienke)

- Coordinates recupling enables for P-wave resonance formation

Strategy of the measurement

The kinetic energy in the K⁻n CM system is:

$$E_{\mathrm{Kn}} \sim -B_n - \left\langle \frac{p^2_{\Lambda\pi}}{2\mu_{\pi,\Lambda,3\mathrm{He}}} \right\rangle$$

recoil energy of the Λπ⁻ pair with respect to the residual

$B_n = 21$ MeV

$< p_3^2/2\mu_{12,3} > \simeq 12$ MeV

see also

A. Cieply et al., Phys. Lett. B 702 (2011) 402,
T. Hoshino et al., Phys. Rev. C 96 (2017) 045204
N. Barnea, E. Friedman, A. Gal, Nucl. Phys. A968 (2017)

Strategy of the measurement

The kinetic energy in the $K^- n$ CM system is:

$$E_{Kn} \sim -B_n - \left\langle \frac{p^2_{\Lambda\pi}}{2\mu_{\pi,\Lambda,3He}} \right\rangle$$

recoil energy of the $\Lambda\pi^-$ pair with respect to the residual

$$B_n = 21 \text{ MeV}$$

$$\langle p_3^2 / 2\mu_{12,3} \rangle \simeq 12 \text{ MeV}$$

so we are testing the interaction about 33 MeV below the KbarN threshold.

The interaction is very short range (off shell dependence on relative momenta is neglected)

$$t_{Kn\to\Lambda\pi}(E_{Kn}) \equiv f^s$$

is a free parameter to be extracted by comparison of predicted and measured momentum probability distributions.

$$\frac{\text{NR}-\text{ar}}{\text{RES}-\text{ar}} = \frac{\int_0^{pmax} P_{ar}^{nr}(p_{\Lambda\pi})\, dp_{\Lambda\pi}}{\int_0^{pmax} P_{ar}^{res}(p_{\Lambda\pi})\, dp_{\Lambda\pi}} =$$

$$= |f_{\text{ar}}^{\text{nr}}|^2 \cdot 8.94 \cdot 10^5 \text{ MeV}^2 .$$

Table 1
Resonant to non-resonant ratios and amplitudes of the various channels extracted from the fit of the $\Lambda\pi^-$ sample. The statistical and systematic errors are also shown. See text for details.

Channels	Ratio/yield	σ_{stat}	σ_{syst}
RES-ar/NR-ar	0.39	$\pm$ 0.04	$^{+0.18}_{-0.07}$
RES-if/NR-if	0.23	$\pm$ 0.03	$^{+0.23}_{-0.22}$
NR-ar	12.0%	$\pm$ 1.7%	$^{+2.0}_{-2.8}$%
NR-if	19.2%	$\pm$ 4.4%	$^{+5.9}_{-3.3}$%
$\Sigma \to \Lambda$ conv.	2.2%	$\pm$ 0.3%	$^{+1.6}_{-0.8}$%
K^{-12}C capture	57.0%	$\pm$ 1.2%	$^{+2.2}_{-3.2}$%

Results of the analysis

$$|f^{nr}_{ar}| = (0.334 \pm 0.018\,\mathrm{stat}^{+0.034}_{-0.058}\mathrm{syst})\ \mathrm{fm}$$

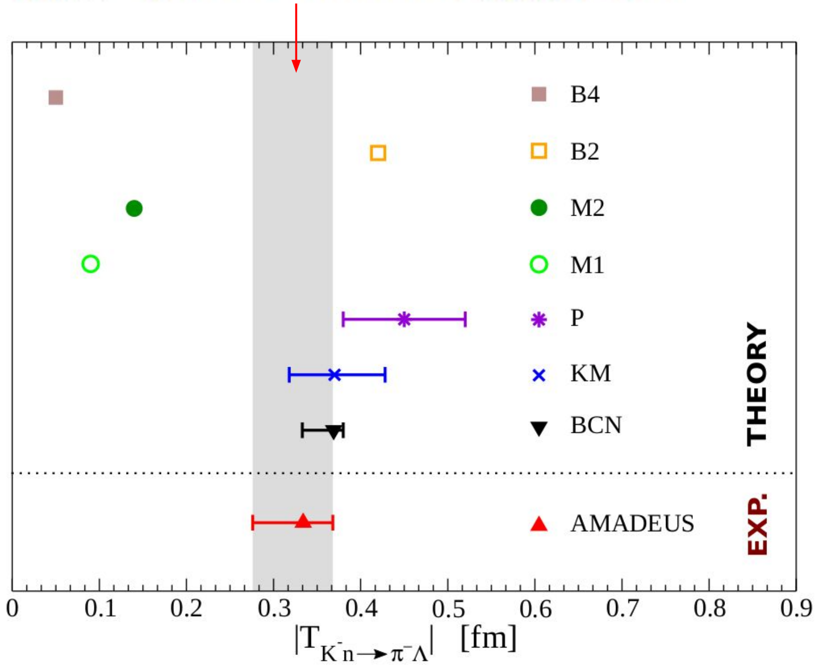

Comparison with theoretically predicted real and imaginary parts of the non resonant, coupled channels, $K^-n \to \Lambda\pi/\Sigma\pi$ scattering amplitudes:

- for each model $|A_{K-n}|$ is calculated at 33 MeV below the KbarN threshold
- $|A_{K-n\to\Lambda\pi^-}|$ is extracted from $|A_{K-n}|$ by calculating the probability ratios:

$$\frac{Prob_{K^-n\to\Lambda\pi^-}}{Prob_{K^-n\to\Sigma^-\pi^0}} = \frac{Ph_{K^-n\to\Lambda\pi^-}}{c_1 Ph_{K^-n\to\Sigma^-\pi^0}}$$

$$\frac{Prob_{K^-n\to\Lambda\pi^-}}{Prob_{K^-n\to\Sigma^0\pi^-}} = \frac{Ph_{K^-n\to\Lambda\pi^-}}{c_2 Ph_{K^-n\to\Sigma^0\pi^-}}$$

Outcome of the measurement

Investigated using: **K⁻ "n"** ^{3}He → **Λπ⁻** ^{3}He

$$|f^{nr}_{ar}| = (0.334 \pm 0.018\,\mathrm{stat}^{+0.034}_{-0.058}\mathrm{syst})\ \mathrm{fm}$$

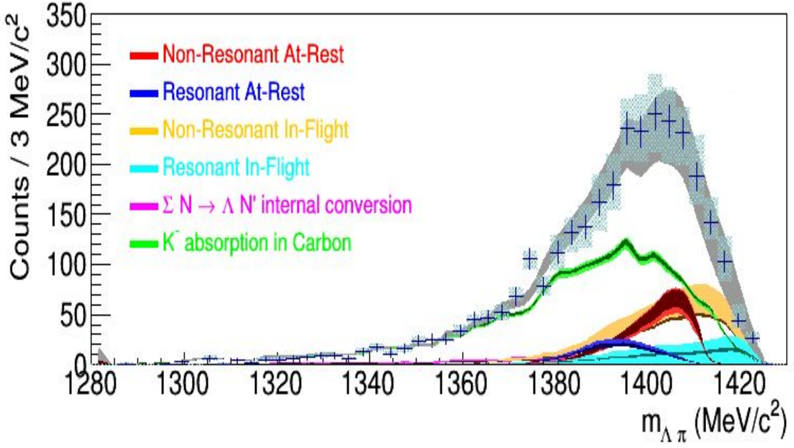

$E = -33$ MeV	$0.334 \pm 0.018\,\mathrm{stat}^{+0.034}_{-0.058}\mathrm{syst}$
$p_{lab} = 120$ MeV	0.33 ± 0.11
$p_{lab} = 160$ MeV	0.29 ± 0.10
$p_{lab} = 200$ MeV	0.24 ± 0.06
$p_{lab} = 245$ MeV	0.28 ± 0.02

TABLE II. The S-wave non-resonant amplitude ($|f^{nr}|$ fm) extracted from $K^-p \to \Lambda\pi^0$ scattering [34, 35] and from this experiment ($E = -33$ MeV).

J. K. Kim, Columbia University Report, Nevis 149 (1966)
J. K. Kim, Phys. Rev. Lett. 19 (1977) 1074

[K. Piscicchia, S. Wycech, L. Fabbietti et al. Phys.Lett. B782 (2018) 339-345]
[K. Piscicchia, S. Wycech, C. Curceanu, Nucl. Phys. A 954 (2016) 75-93]

YN correlation studies

K⁻ multi-nucleon absorptions are investigated by reconstructing the **hyperon-nucleon/nuclei** emitted in the final state of the process (i.e. Λp, Σ^0p, and Λt final states)

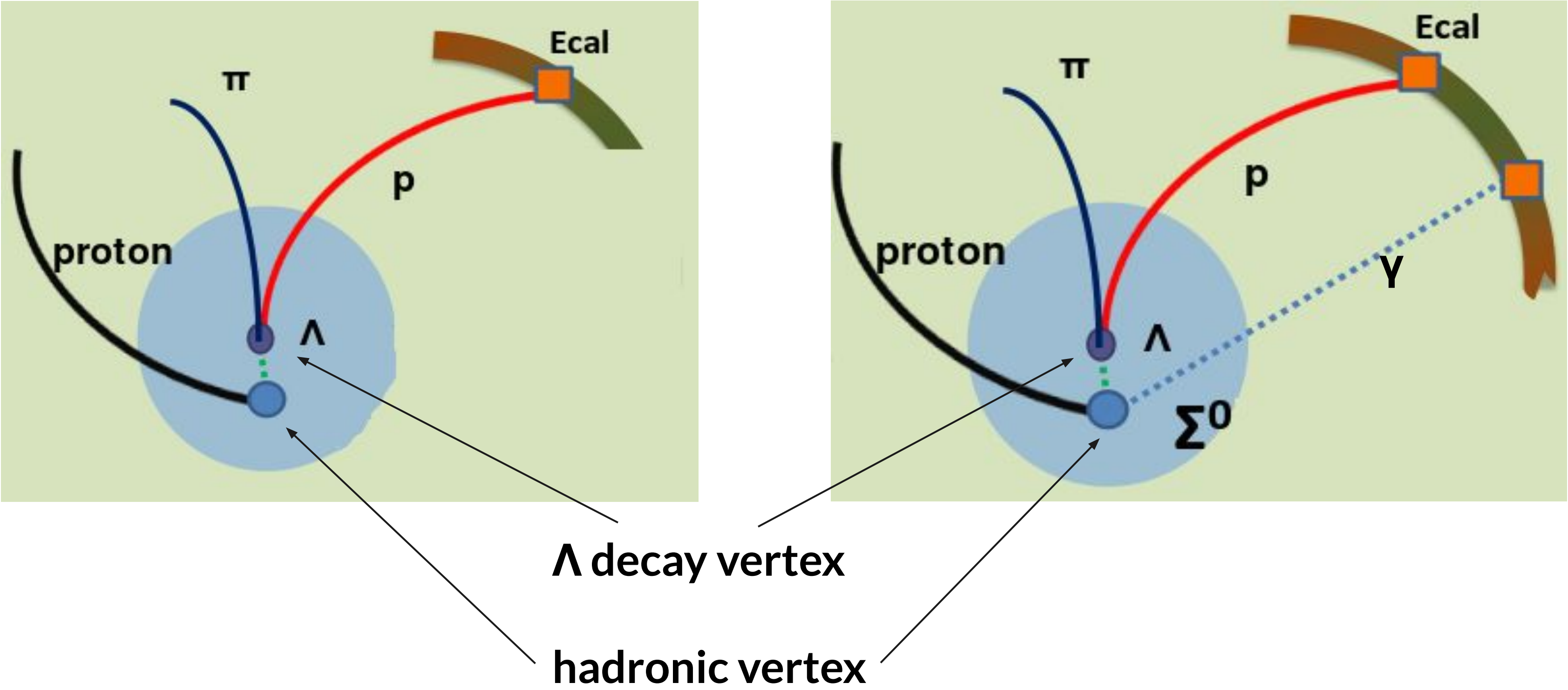

$\Sigma^0 p$ analysis: $K^- + {}^{12}C \rightarrow \Sigma^0 + p + R$

Simultaneous fit of:

- $\Sigma^0 p$ invariant mass;
- angular correlation;
- proton momentum;
- Σ^0 momentum.

Total reduced χ^2: $\chi^2/dof = 0.85$

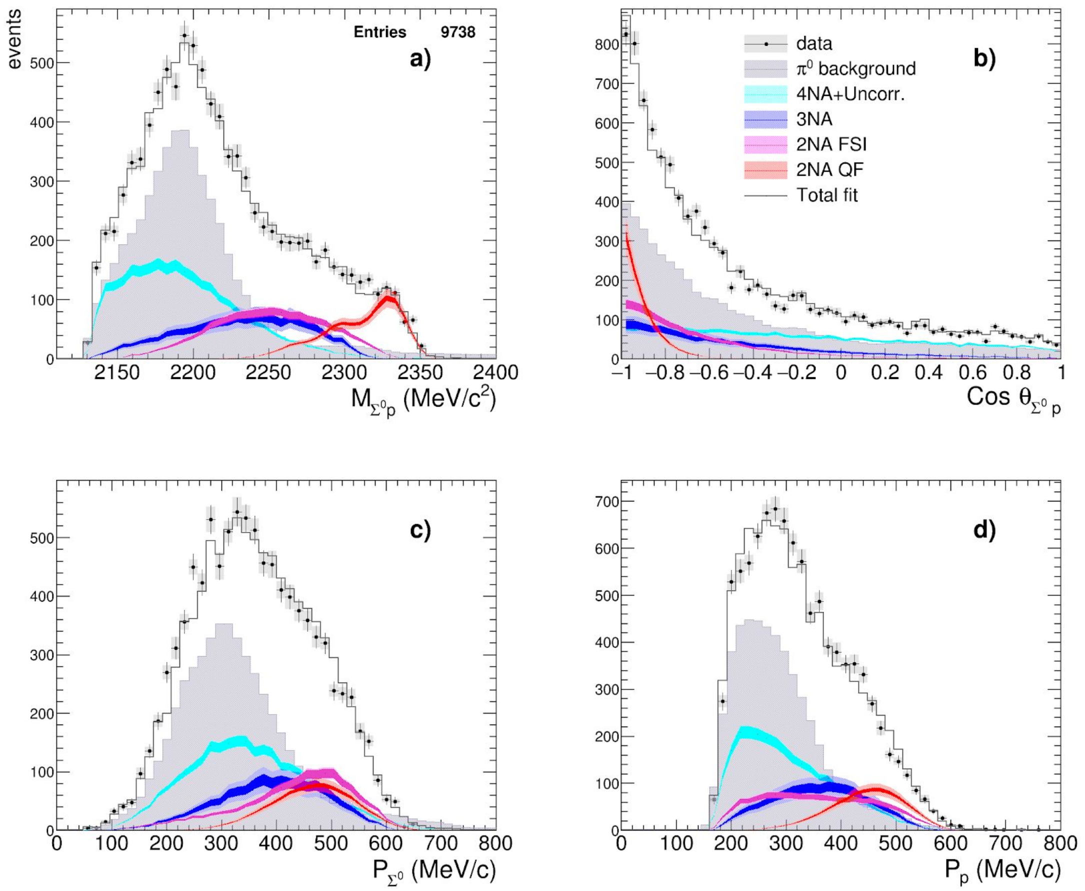

[O. Vazquez Doce, L. Fabbietti et al., Phys.Lett. B 758, 134-139 (2016)]

$\Sigma^0 p$ analysis: $K^- + {}^{12}C \rightarrow \Sigma^0 + p + R$

Simultaneous fit of:

- $\Sigma^0 p$ invariant mass;
- angular correlation;
- proton momentum;
- Σ^0 momentum.

Total reduced χ^2: $\chi^2/dof = 0.807$

Best solution:
(best χ^2 and higher yield)

- B = 45 MeV/c²
- Γ = 30 MeV/c²

Statistical significance of 1σ
(evaluated by means of F-test method)

[O. Vazquez Doce, L. Fabbietti et al., Phys.Lett. B 758, 134-139 (2016)]

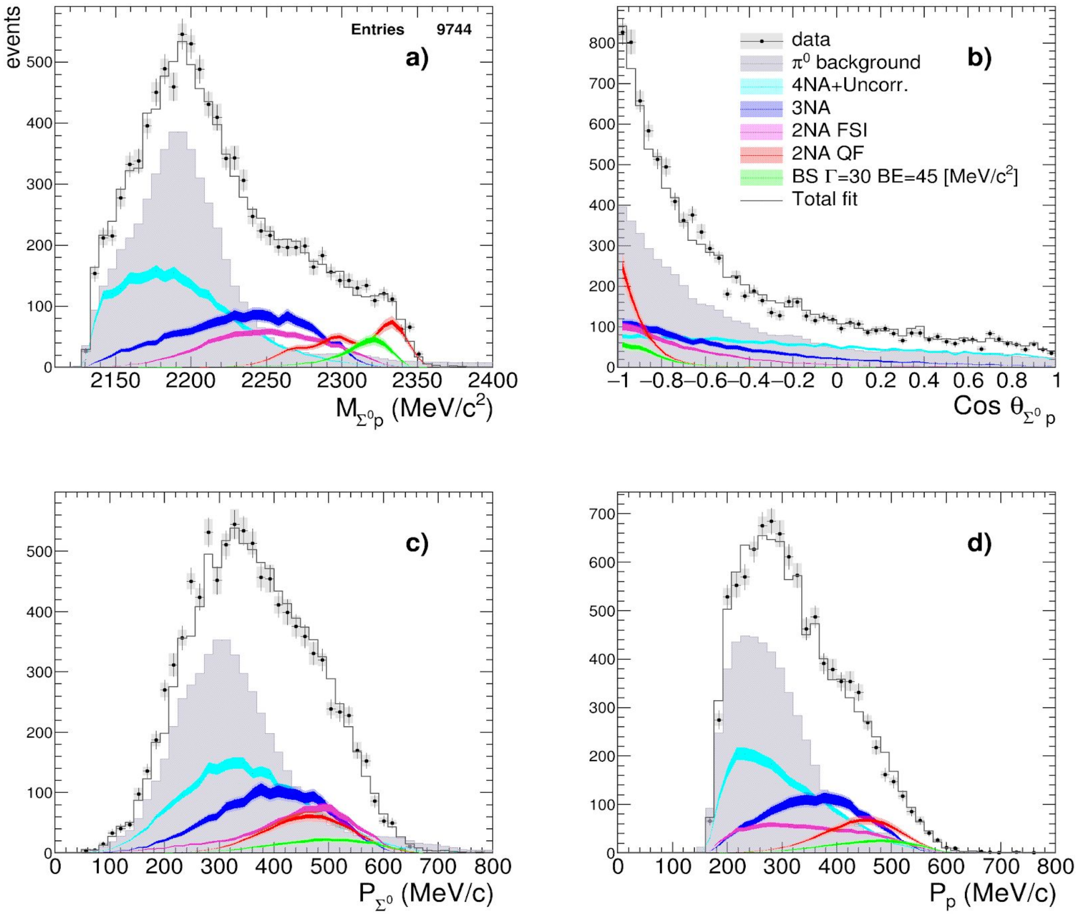

- in black the invariant mass m_{ij} for each couple of clusters selected by χ^2_t,
- in green the invariant mass m_{12} of the photons $\gamma_1 - \gamma_2$ selected by $\chi^2_{\pi\Sigma}$,
- in red the invariant masses m_{13} and m_{23} of the "wrong" couples.

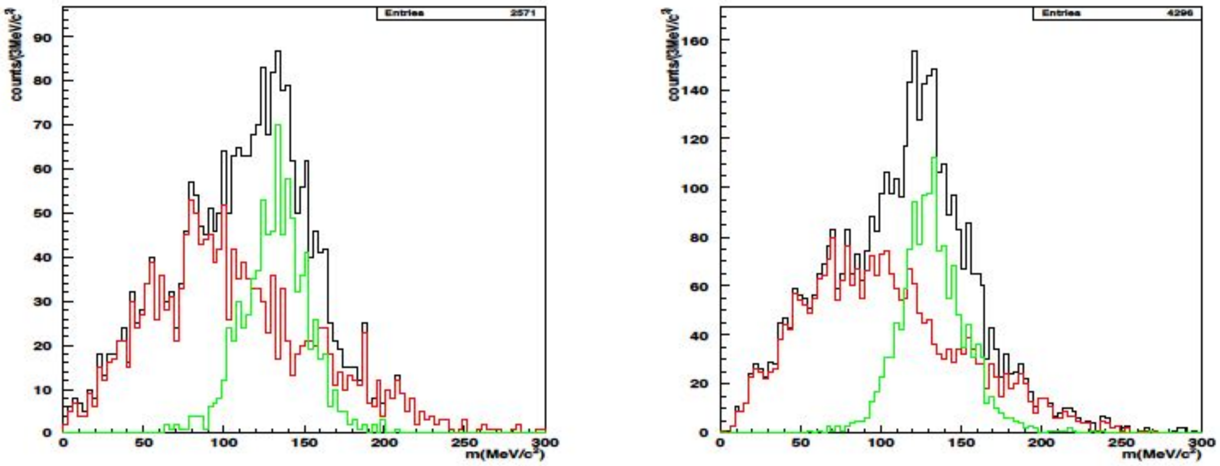

Figure 3.12: The plot illustrates the invariant mass of various combinations of three photons, as explained in the text, for pure signal MC events left and data right.

Calculation of the if reaction requires as input the negative kaon momentum, which is sampled according to the true MC (i.e. not passed for the events reconstruction) momentum distribution of the negative kaons inside the DC volume.

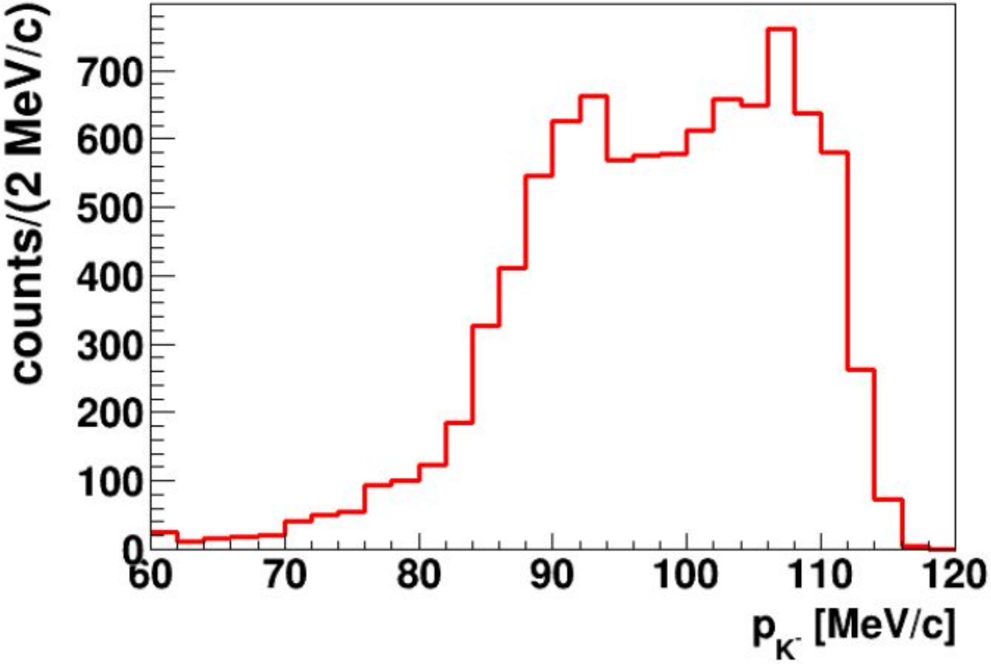

Calculated distributions $\Lambda\,\pi^0$

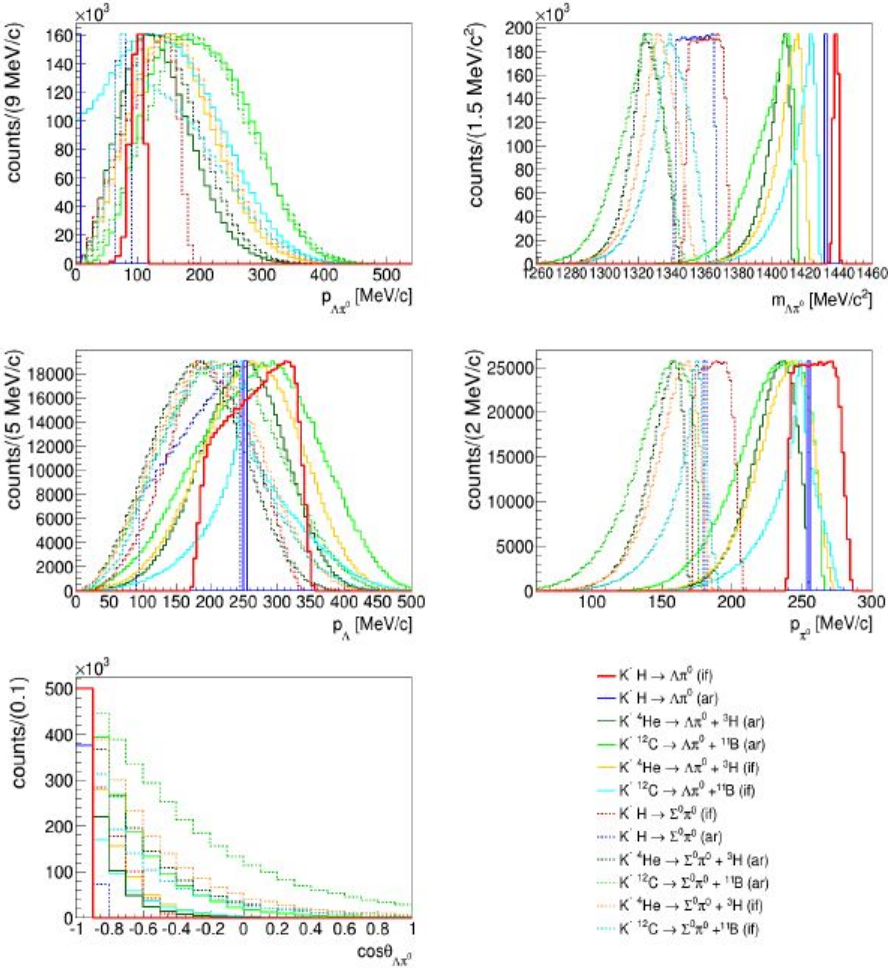

Calculated distributions Σ^0 π^0

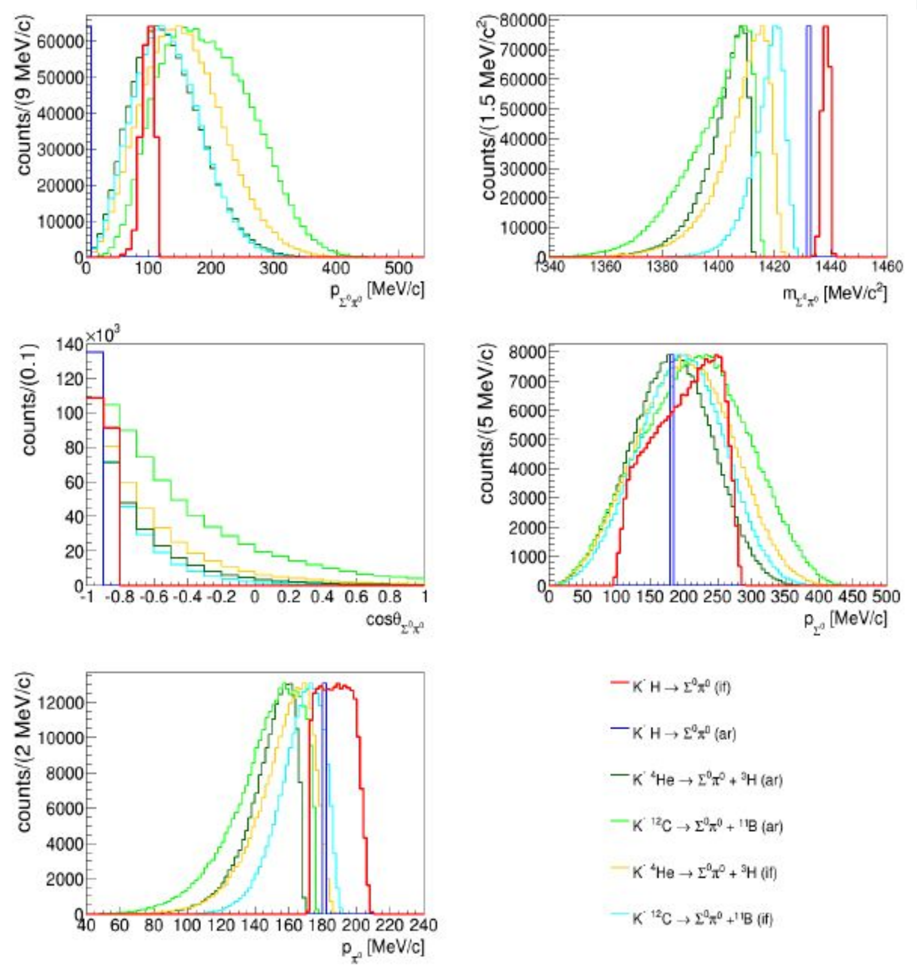

Reconstructed MC distributions $\Lambda\pi^0$

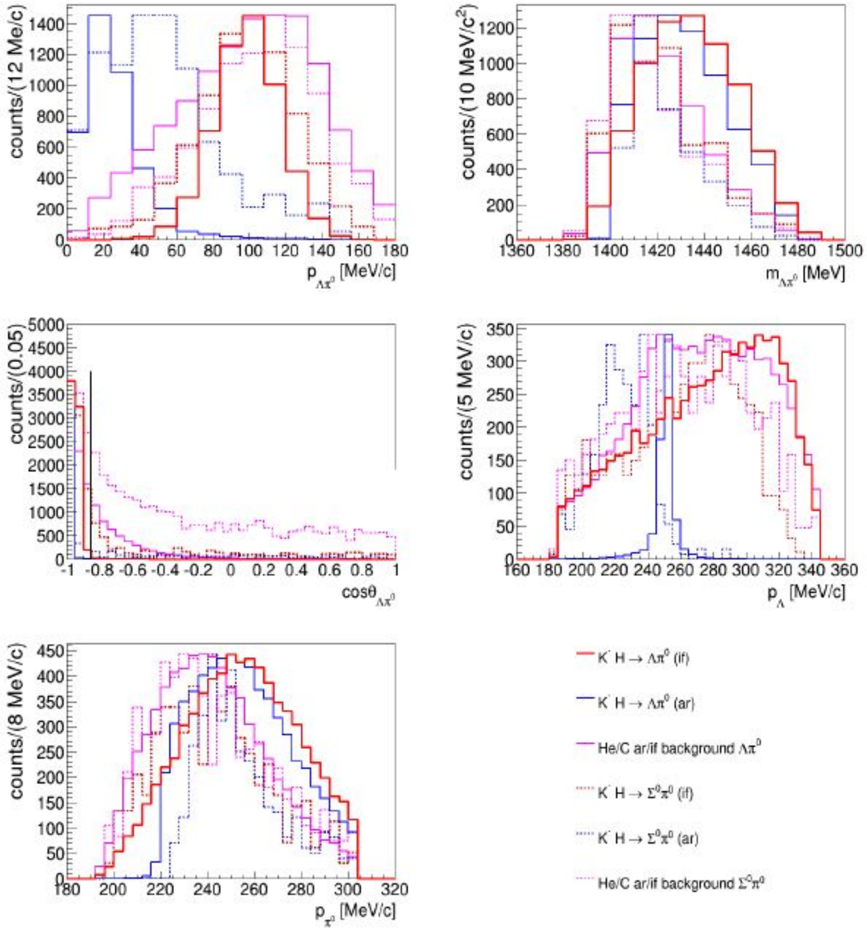

Figure 18. Reconstructed MC distributions: total $\Lambda\pi^0$ momentum (top left), $\Lambda\pi^0$ invariant mass (top right), $\cos\theta_{\Lambda\pi^0}$ (middle left), Λ momentum (middle right), π^0 momentum (bottom left), the cut corresponding to $\cos\theta_{\Lambda\pi^0}$<-0.85 is represented as a dark green line. The color legend is shown in the bottom right panel. The same events selection as for the data is applied.

Reconstructed MC distributions $\Sigma^0\,\pi^0$

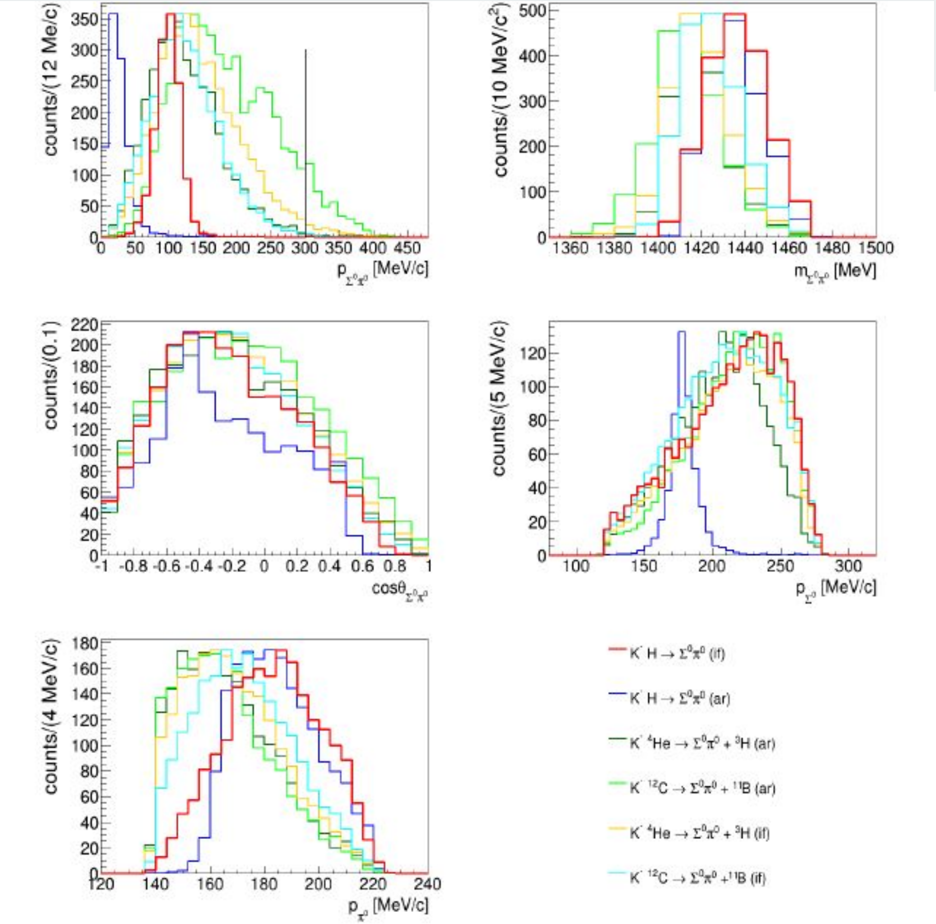

Figure 10. Reconstructed MC distributions: total $\Sigma^0\pi^0$ momentum (top left), the cut corresponding to $p_{\Sigma^0\pi^0} < 300$ MeV/c is represented as a dark green line, $\Sigma^0\pi^0$ invariant mass (top right), $\cos\theta_{\Sigma^0\pi^0}$ (middle left), Σ^0 momentum (middle right) and π^0 momentum (bottom left). The color legend is shown in the bottom right panel. The same events selection as for the data is applied.

5.1 Consistency check of the measured spectra with the fit results

Following the suggestion of the referees, in order to test self-consistency of the fit results with the measured distributions of those variables which most severely affected the selection cuts, we show in this Section the comparisons among measured and simulated $m_{\Lambda\gamma_3}$, $m_{\gamma_1\gamma_2}$ and χ^2_m as they result from the fit of the data. The comparison is performed normalising the MC distributions to the data, then weighting each contribution with the corresponding parameter obtained from the fit (Table 1). The adopted colour code is the same used in Fig. 13. Black points represent the data, error bars correspond to the statistical errors, the systematic errors are light blue boxes. The gray distributions are given by the sum of the coloured distributions. The plots show a satisfactory agreement between MC and data.

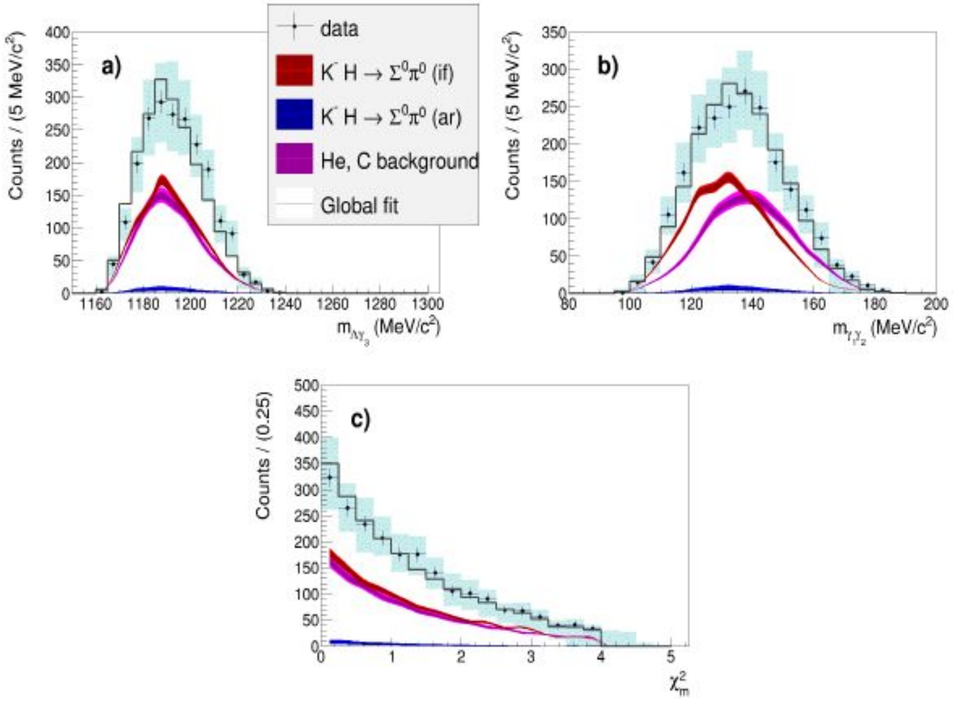

Determination of the $K^- p \to \Sigma^0\pi^0$ cross section by means of the simultaneous fit of the $(p_{\Lambda\pi^0}, m_{\Lambda\pi^0}, p_\Lambda$ and $p_{\pi^0})$ variables

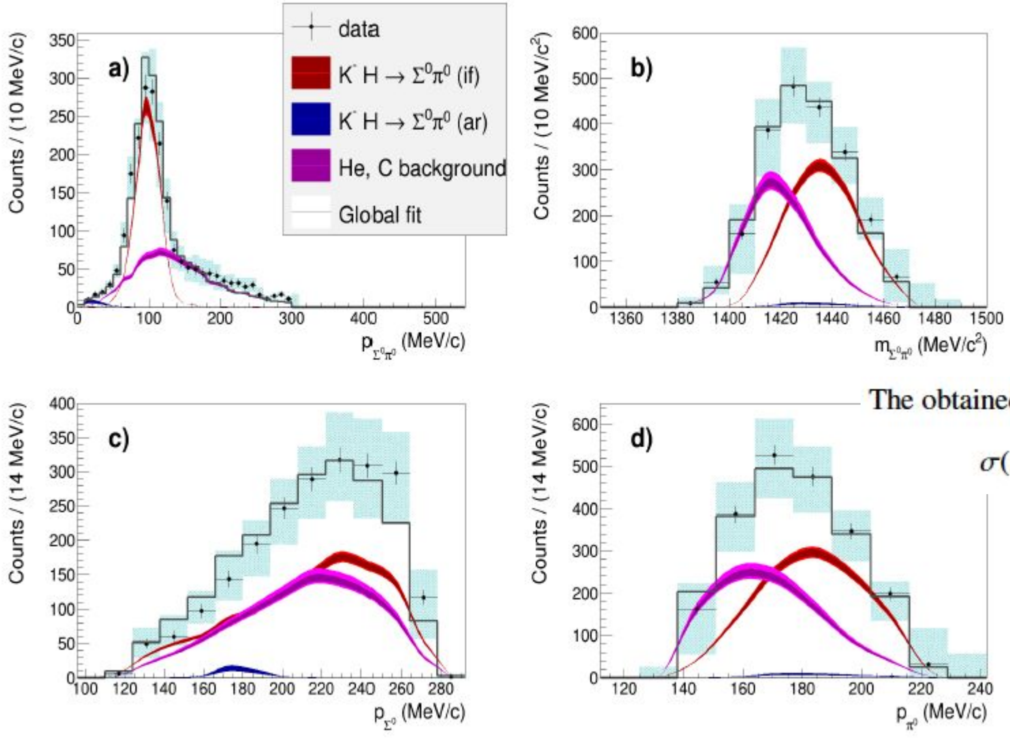

The obtained cross section is:

$$\sigma(K^- p \to \Sigma^0\pi^0)(p_K = (98 \pm 10)MeV/c) = 44.9 \pm 1.4(stat.)^{+2.3}_{-2.1}(syst.)\text{ mb}$$

Figure 23. Simultaneous fit of $p_{\Sigma^0\pi^0}$ (left upper), $m_{\Sigma^0\pi^0}$ (right upper), p_{Σ^0} (left lower) and p_{π^0} (right lower). Black points represent the data, error bars correspond to the statistical errors, the systematic errors are light blue boxes. The gray line distributions represent the global fitting function. Coloured lines represent MC simulations with final selection applied weighted with parameters obtained from the fit. The dark and light bands correspond to statistical and systematic errors, respectively.

Cross section calculation

$$\sigma = \frac{N^{tag}_{reaction}}{N^{tag}_{projectiles} \cdot n \cdot L}$$

$$N^{tag}_{reactions} = \frac{\alpha \cdot N^{\Sigma^0\pi^0}_{obs} \cdot A_{tag}}{\epsilon \cdot BR_{\Lambda \to p\pi^-}}$$

number of impinging K-

corrected for the decay

mean path length crossed by the K-

which accounts for the K- impinging angle (angle between the tangent vector to the particles trajectory at the entrance point and the radial direction)

$$n = 10 \frac{N_{AV}}{A} \cdot \rho$$

Systematic errors

The systematic errors are determined by repeating several times the same fit procedure, by varying independently all the analysis cuts which were optimized for the $\Sigma^0\pi^0$ and $\Lambda\pi^0$ samples selection (see Sections III and IV). The systematic error on the i-th parameter of the fit, due to a variation of the j-th cut, is defined as:

$$\sigma^{j}_{sist,i} = \alpha^{j}_{i} - \alpha_i \qquad (4)$$

Total, positive and negative systematic errors are obtained by summing in quadrature the positive and negative systematic fluctuations.

With the exception of those quantities for which the statistical error is known (e.g. $m_{\gamma_1\gamma_2}$, $m_{\Lambda\gamma 3}$ and $\cos\theta_{\Lambda\pi^0}$), in which case the systematics are evaluated by applying 1σ fluctuations to the corresponding cuts, and of the background sources whose contribution is known by simulations (e.g. the background introduced by the ρ_Λ cut), for the other selections we chose to change the cuts of the amount necessary to increase (or decrease) the selected number of events of 15%, with respect to the standard. This is the case of the constraints on χ^2_t, $\chi^2_{m_{\gamma_1\gamma_2}}$ and $\chi^2_{m_{\Lambda\gamma_3}}$, and of the phase space selections in the $p_{\pi^0} - p_{\Sigma^0}$ and in the $p_{\pi^0} - p_\Lambda$ planes. The systematic uncertainty introduced by setting equal contributions of K^- absorptions on Helium and Carbon, both for the *ar* and *if* processes, is set by performing 15% variations of the relative contribution of each process.

The $p_{\Sigma^0\pi^0}$ constraint was optimized based on a scan in the range $(280 \div 350)$ MeV/c, in steps of 10 MeV/c (corresponding to the resolution $\sigma_{p_{\Sigma^0\pi^0}}$) yielding the minimum reduced χ^2 for $p_{\Sigma^0\pi^0} = 300$ MeV/c. The contribution to the systematic errors is obtained by the condition $p_{\Sigma^0\pi^0} < 310$ MeV/c.

The systematics introduced by the decay correction in the N_{K^-} calculation and by the evaluation of L are estimated by doubling the 1 cm step length, and diminishing of 15% the number of simulated kaons.

Negligible contributions in the $\Lambda\,\pi^0$ fit

4. $K^- + H \quad \rightarrow \quad \Sigma^0 + \pi^0$ at-rest (dashed red);

5. $K^- + H \quad \rightarrow \quad \Sigma^0 + \pi^0$ in-flight (dashed blue);

6. $K^- + {}^4He/{}^{12}C \quad \rightarrow \quad \Sigma^0 + \pi^0 + {}^3H/{}^{11}B$, weighting with the same probability the ${}^4He$ and ${}^{12}C$, at-rest and in-flight captures (dashed magenta).

The contributions of the processes 5 and 6 are found to be negligibly small. The K^- ${}^4He/{}^{12}C$ $\rightarrow \Sigma^0\pi^0$ reactions followed by the Σ^0 decay overlap over broad ranges of the phase space with the same reactions with direct $\Lambda\pi^0$ production; if the cross section is set to the value obtained in Section 6, using the efficiency for the detection of a $\Lambda\pi^0$ final state corresponding to the process K^- H $\rightarrow \Sigma^0\pi^0 \rightarrow \Lambda\gamma\pi^0$ this process is found to contribute 0.009 to the measured total number of events, the fit is not sensitive to this contribution. According to the measurement described in Ref. [27] in which the processes of

$p_{\pi 0}$ **resolution**: $\sigma \approx 12$ MeV/c

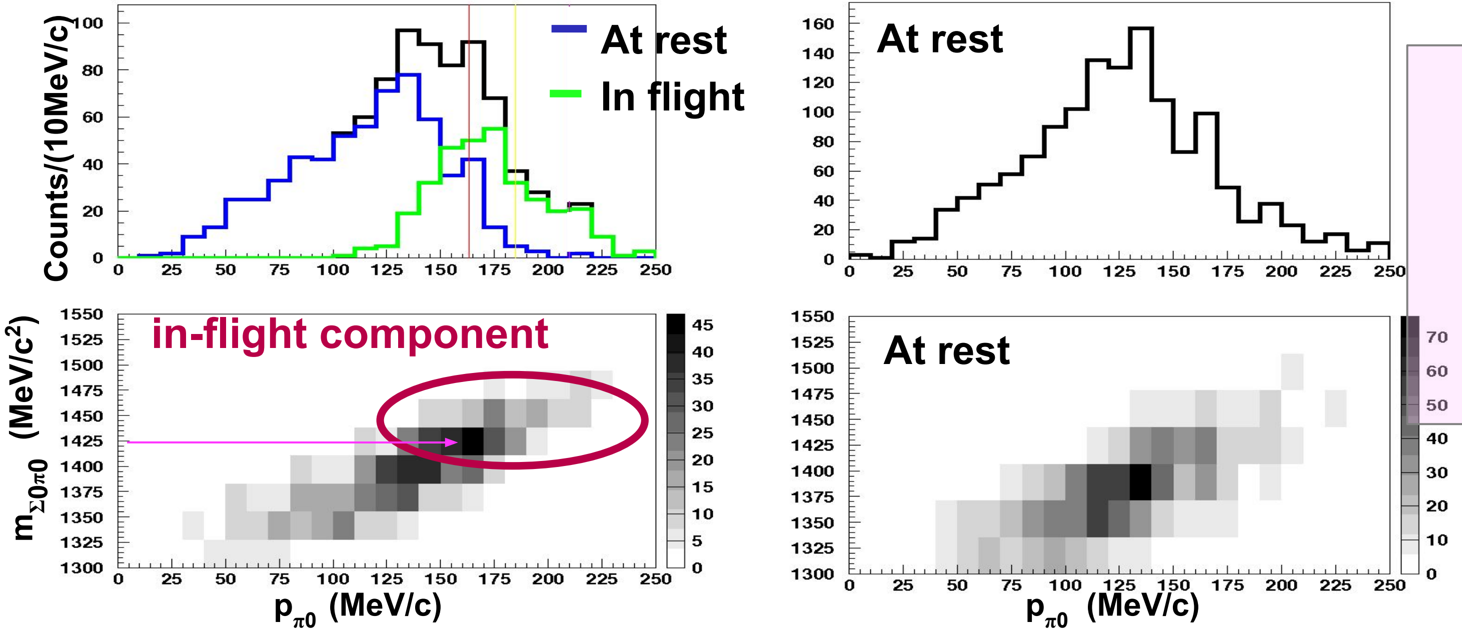

IN-FLIGHT

K- 12C

opens a window

between 1416 MeV

and K-Nth

difficulty: epoxy resin, contained in the carbon fibre target, contains H

BUT - **K^-H interaction probability, based on K^- interaction AT-REST in hydrocarbons mixture data (Lett. Nuovo Cimento, C 1099 (1972)) gives max contribution order of 1% !!!**

HYDROGEN contamination → from $\Sigma^+ \pi^-$

$K^- p \rightarrow \Sigma^+ \pi^-$ detected via: $(p\pi^0)\, \pi^-$

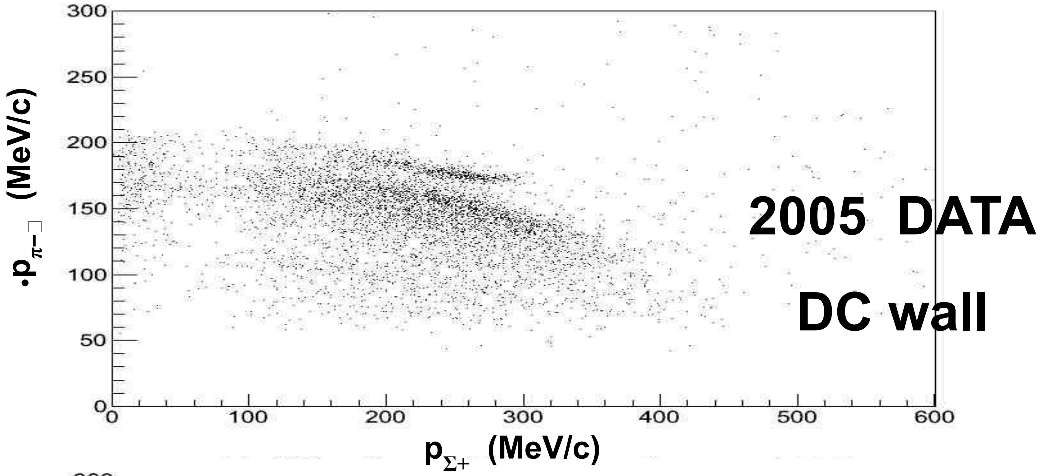

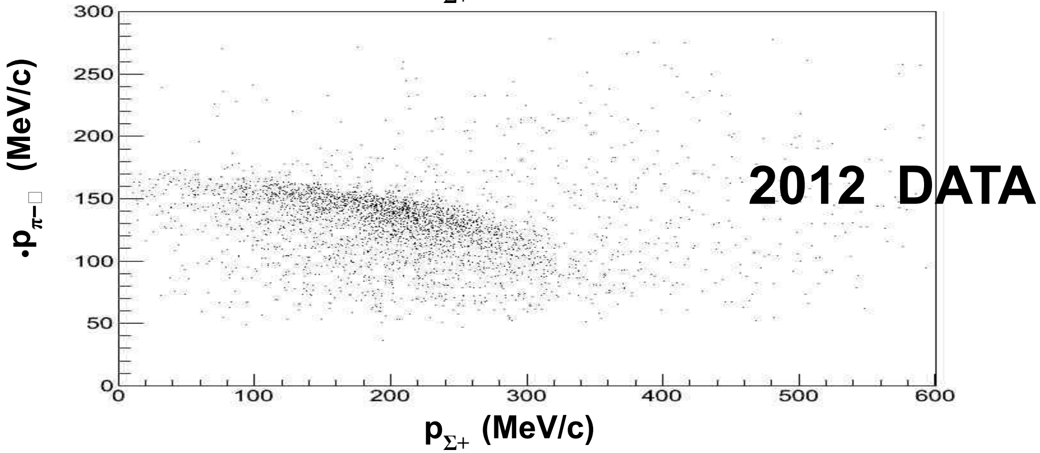

NOW

Thanks to the good p_{π^-} resolution

= 1 MeV

HYDROGEN contamination → from $\Sigma^+ \pi^-$

$K^- p \rightarrow \Sigma^+ \pi^-$ detected via: $(p\pi^0)\,\pi^-$

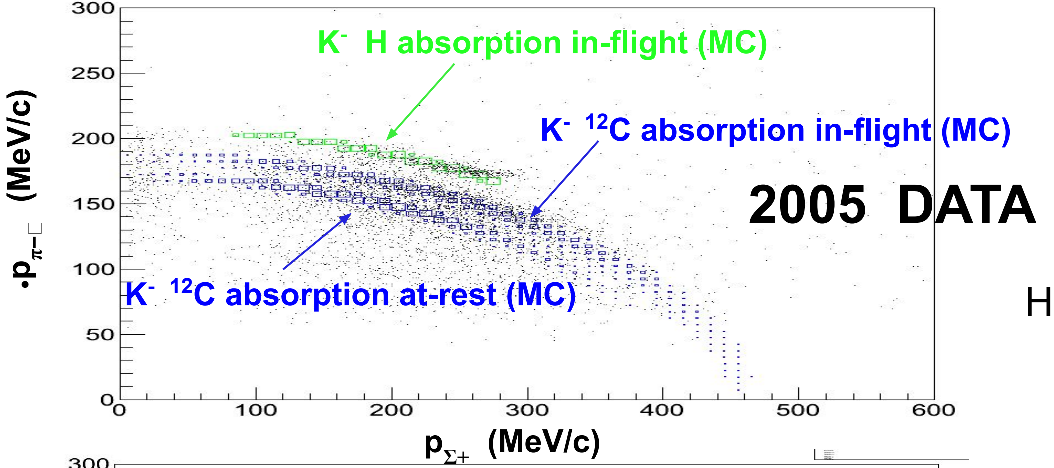

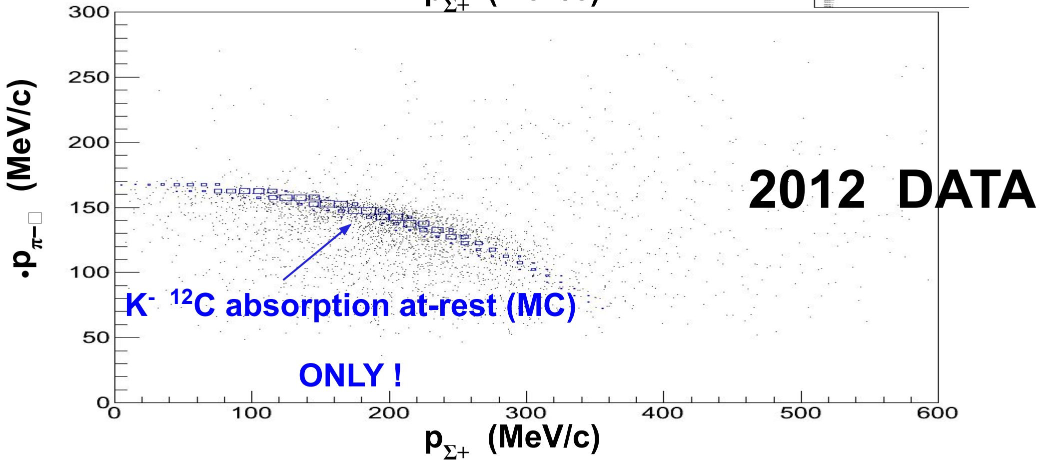

K^- H contribution ~ 20%

H atoms in the molecules mainly contribute to **K- H absorption in-flight**, resulting in a **non-resonant background in the $\Sigma^0 \pi^0$ spectra**

probability of K- H capture at rest

To conclude this section we will estimate the contribution of K^--nuclear absorptions on Hydrogen from isobutane molecules. In [45] the probability of K^- absorptions on Hydrogen in a mixture of hydrocarbons was measured and found to be as low as (0.040 ± 0.004). The mixture composition was:

$$24.7\% \, C_2H_6 \ , \ 73.9\% \, C_3H_8 \text{ and } 1.3\% \, C_4H_{10}. \tag{5.6}$$

We weighted the measured probability taking into account for the Hydrogen content of the mixture adopted in [45] with respect to the pure isobutane case, and for the volume ratio of isobutane in the KLOE DC. The probability of K^- capture on Hydrogen in the drift chamber results to be 0.0028 ± 0.0003. The

[45] C. Vander Velde-Wilquet et al., Nuovo Cimento, Lett. 5, (1972) 1099.

Total BR of the K^- 2NA process in ^{12}C

Hyperon-nucleon pairs produced in K^-2NA process: **Λp Λn Σ^0p Σ^0n Σ^+n Σ^-p Σ^-n**

BCN calculation at 0.3 ρ_0 (baryon density in ^{12}C) → BR(K^-2NA → YN) = (15.4 ± 2.2) %

[J. Hrtánková and A. Ramos. Phys. Rev. C, 101(3):035204, 2020]

Process	Branching Ratio (%)
2NA-QF Λp	0.25 ± 0.02 (stat.) $^{+0.01}_{-0.02}$(syst.)
2NA-FSI Λp	6.2 ± 1.4(stat.) $^{+0.5}_{-0.6}$(syst.)
2NA-QF Σ^0p	0.35 ± 0.09(stat.) $^{+0.13}_{-0.06}$(syst.)
2NA-FSI Σ^0p	7.2 ± 2.2(stat.) $^{+4.2}_{-5.4}$(syst.)
2NA-CONV Σ/Λ	2.1 ± 1.2(stat.) $^{+0.9}_{-0.5}$(syst.)
3NA Λpn	1.4 ± 0.2(stat.) $^{+0.1}_{-0.2}$(syst.)
3NA Σ^0pn	3.7 ± 0.4(stat.) $^{+0.2}_{-0.4}$(syst.)
4NA Λpnn	0.13 ± 0.09(stat.) $^{+0.08}_{-0.07}$(syst.)
Global Λ(Σ^0)p	21 ± 3(stat.) $^{+5}_{-6}$(syst.)

We measure a total K^-2NA BR in ^{12}C

→ (16.1 ± 2.9(stat.) $^{+4.3}_{-5.5}$ (syst.))%,

Λp and Σ^0p pairs in the final state....
....information on the remaining YN pairs provided by FSI e Conversion reactions

[R. Del Grande, K. P., et al., 2020 Phys. Scr.95 084012]

Total BR of the K^- 2NA process in ^{12}C

FSI and Conversion reactions contributing to the measured BRs

	primary interaction	secondary interaction
2NA-FSI Λp	$K^- pn \rightarrow \Lambda\, n$	$\Lambda\, p \rightarrow \Lambda\, p$
	$K^- pn \rightarrow \Lambda\, n$	$n\, p \rightarrow n\, p$
	$K^- pp \rightarrow \Lambda\, p$	$\Lambda\, N \rightarrow \Lambda\, N$
	$K^- pp \rightarrow \Lambda\, p$	$p\, N \rightarrow p\, N$
2NA-FSI $\Sigma^0 p$	$K^- pn \rightarrow \Sigma^0\, n$	$\Sigma^0\, p \rightarrow \Sigma^0\, p$
	$K^- pn \rightarrow \Sigma^0\, n$	$n\, p \rightarrow n\, p$
	$K^- pp \rightarrow \Sigma^0\, p$	$\Sigma^0\, N \rightarrow \Sigma^0\, N$
	$K^- pp \rightarrow \Sigma^0\, p$	$p\, N \rightarrow p\, N$
2NA-Conv.	$K^- pn \rightarrow \Sigma^0\, n$	$\Sigma^0\, p \rightarrow \Lambda\, p$
	$K^- pp \rightarrow \Sigma^0\, p$	$\Sigma^0\, p \rightarrow \Lambda\, p$
	$K^- pp \rightarrow \Sigma^0\, p$	$\Sigma^0\, n \rightarrow \Lambda\, n$
	$K^- pn \rightarrow \Sigma^-\, p$	$\Sigma^-\, p \rightarrow \Lambda\, n$
	$K^- pp \rightarrow \Sigma^+\, n$	$\Sigma^+\, n \rightarrow \Lambda\, p$

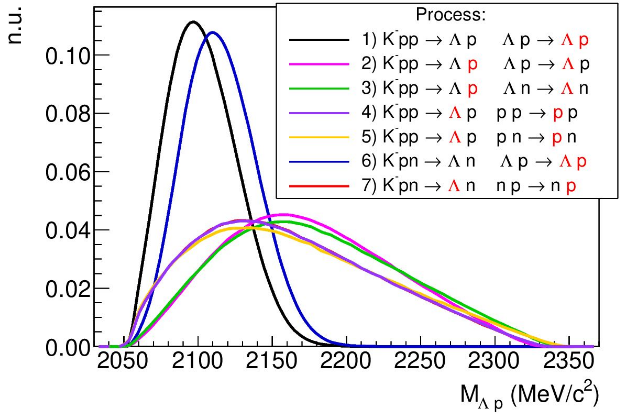

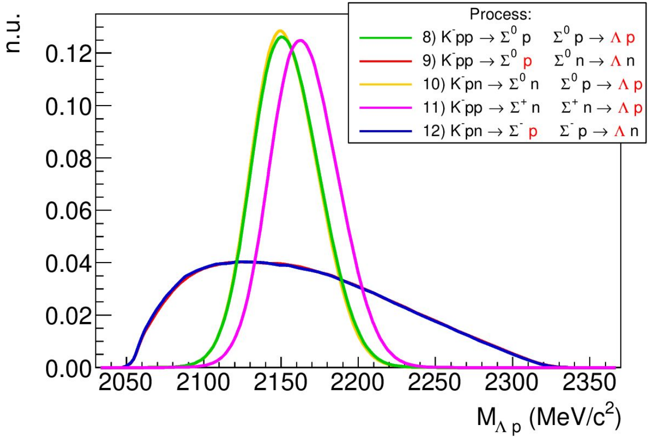

red = detected Λp pair

K^-pp search in K^- induced reactions

FINUDA at DAΦNE: $K^-_{stop} + X \rightarrow \Lambda + p + X'$

only back-to-back Λp pairs ($\cos\theta_{\Lambda p} < -0.8$) **detected particles**

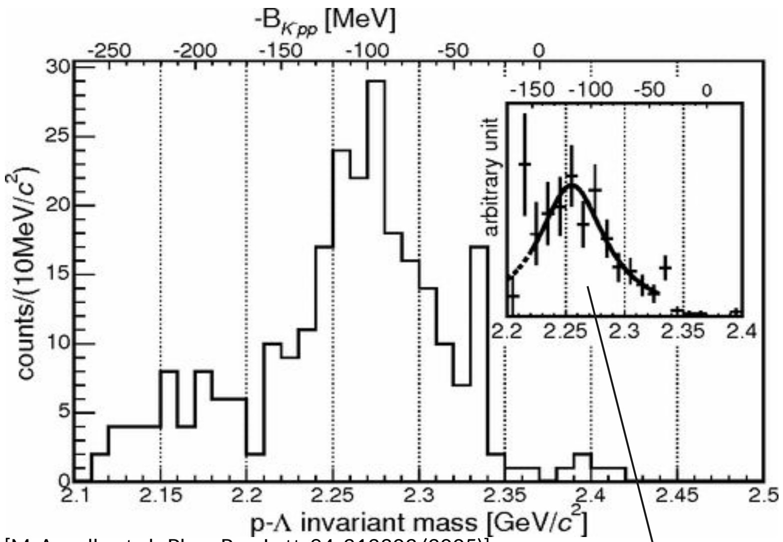

[M. Agnello et al., Phys. Rev. Lett. 94, 212303 (2005)]

Interpreted as the signal of:
$K^-pp \rightarrow \Lambda + p$

extracted parameters:

BE = $(115^{+6}_{-5}\,(\text{stat.})^{+3}_{-4}\,(\text{syst.}))$ MeV

$\Gamma = (67^{+14}_{-11}(\text{stat.})^{+2}_{-3}(\text{syst.}))$ MeV/c^2

E549 at KEK: $K^-_{stop} + {}^4He \rightarrow \Lambda + p + X'$

detected particles

[T. Suzuki et al., Mod. Phys. Lett. A23 (2008) 2520-2523.]

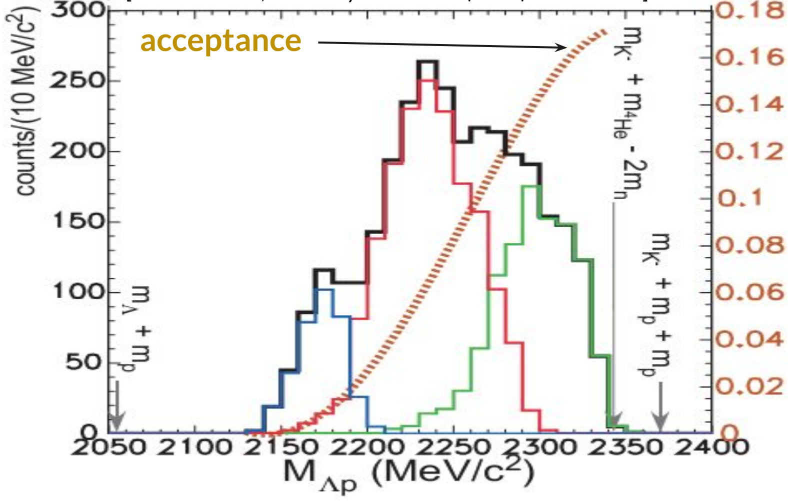

Using the missing mass information, three components to the invariant mass spectrum are found:

- **1NA**: K^- single nucleon absorption
- **2NA**: K^- two nucleon absorption
- **2NA + conversion**, **multi-nucleon**, **or Bound State**?

3NA (K$^-$ ppn) + n $\rightarrow$ Σ^0 d + n wo FSI

- clean mometum mass correlation

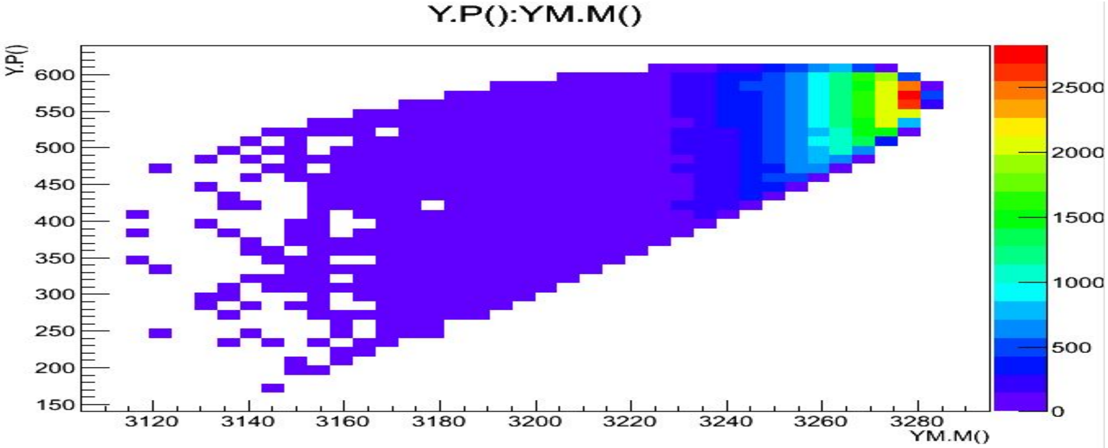

MC

$p_{\Sigma 0}$ vs $m_{\Sigma 0d}$

DATA K$^-$ ^{12}C

$p_{\Sigma 0}$ vs $m_{\Sigma 0d}$

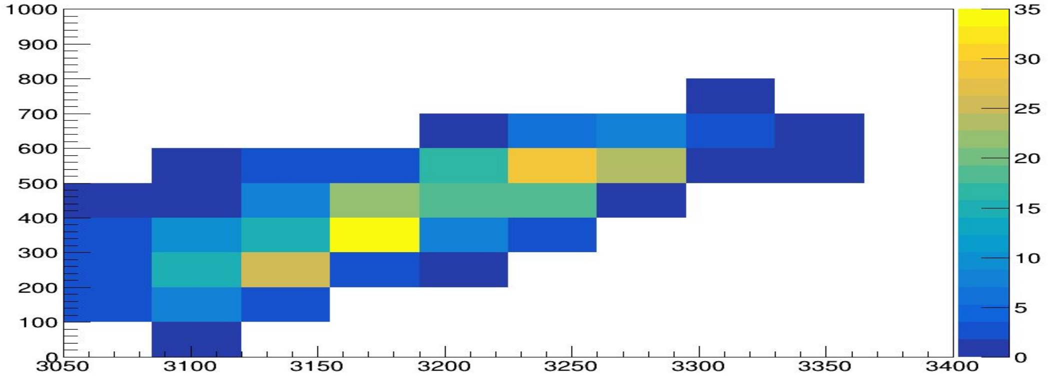

3NA - (K- ppn) + n → Σ0 d + n signature:

Highest Σ0 - d angular correlation - low Fermi momentum neutron

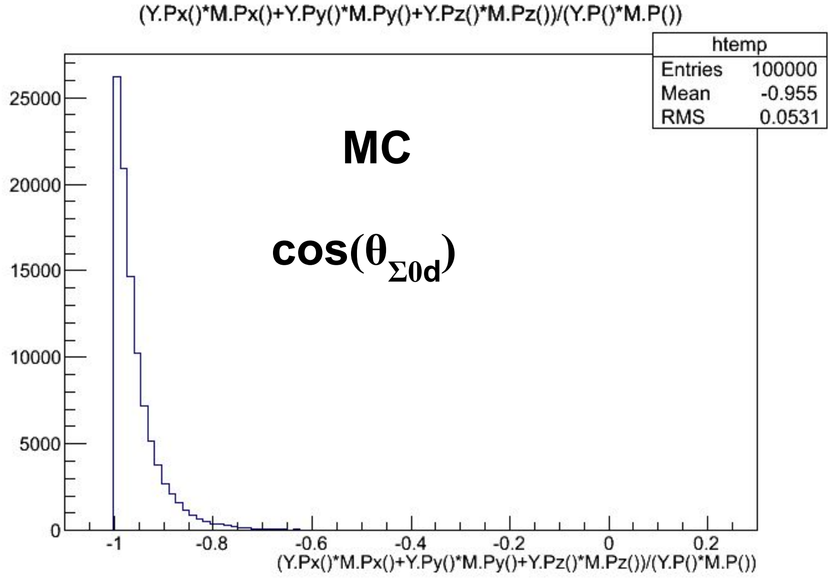

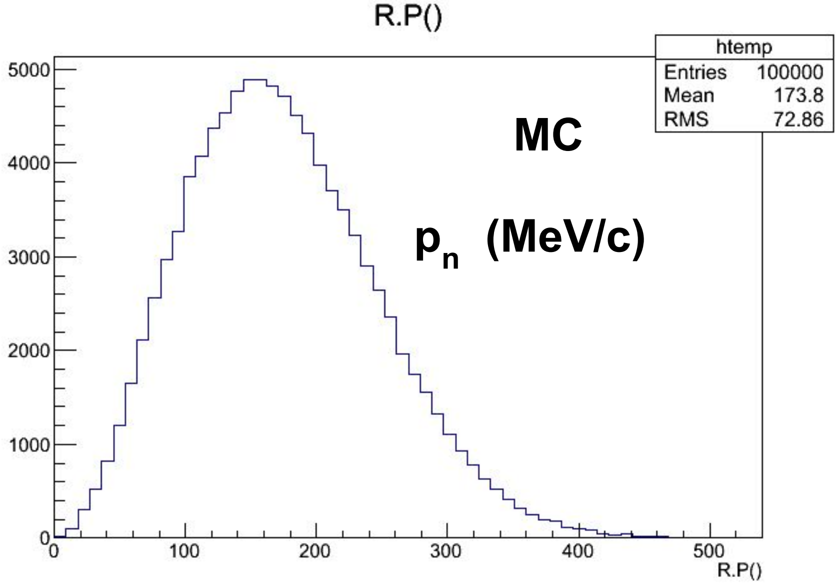

Involved reactions - background:

2NA - $(K^- pn) + d \rightarrow \Sigma^0 n + d$

+

2 possible elastic FSI

1) $n\, d \rightarrow n\, d$ we may take advantage of the well known σ_{NN} data

2) $\Sigma^0\, d/n \rightarrow \Sigma^0\, d/n$ *well separated in the lower energy part of the final state phase space*

2NA

- (K- pn) + d → Σ0 n + d
- lower invariant mass

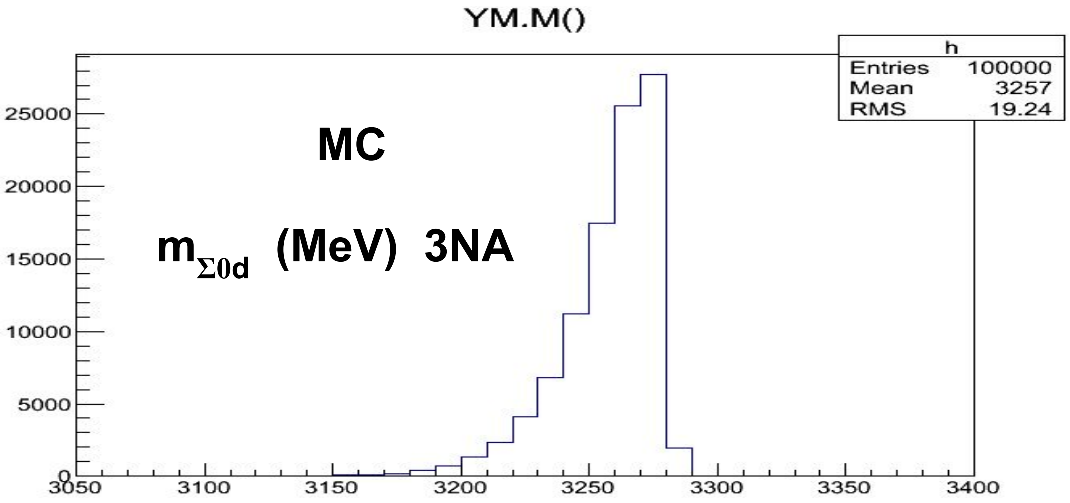

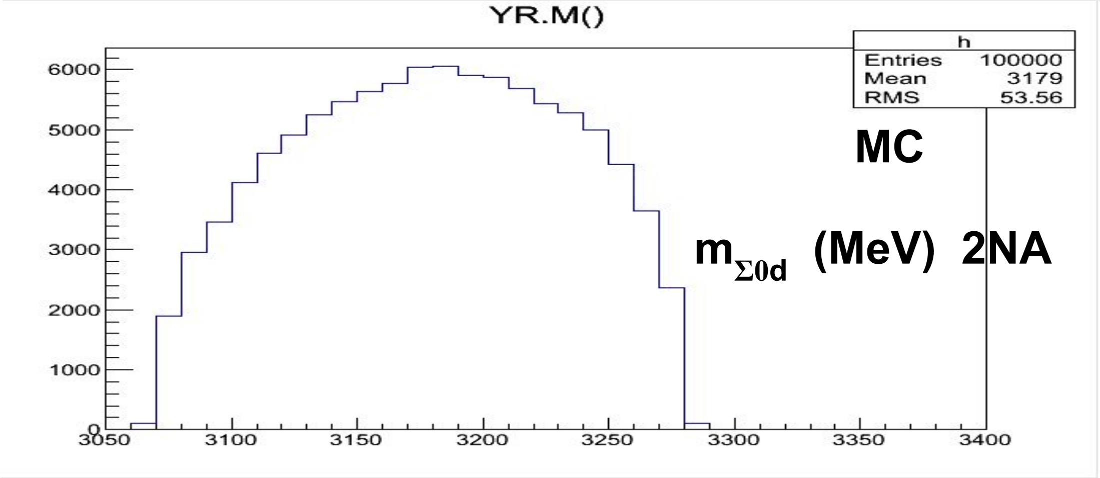

2NA

- $(K^- pn) + d \rightarrow \Sigma^0\, n + d$
- high momentum neutrons

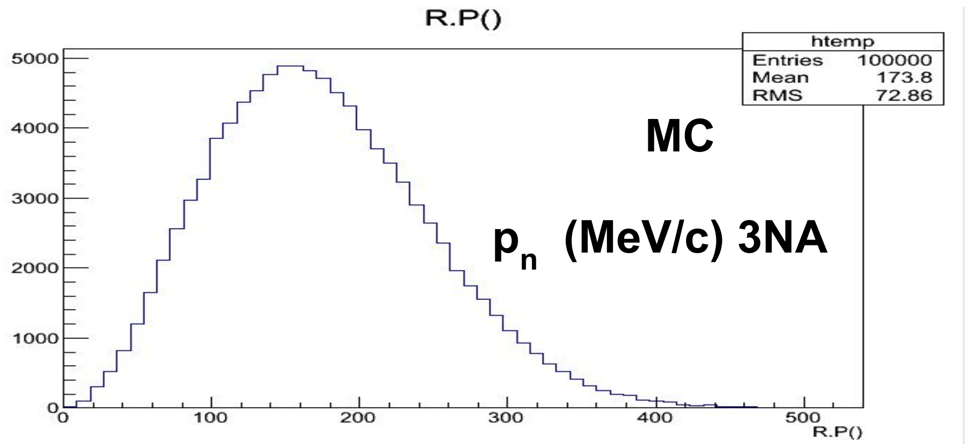

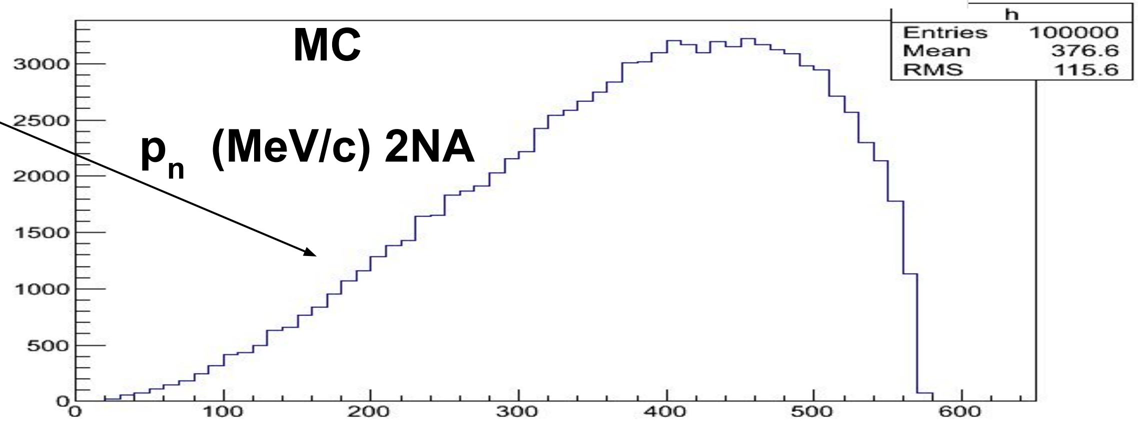

Detection of neutrons will be crucial for a clean separation of 3NA with respect to 2NA.

Involved reactions - background:

1NA - $(K^- p) + pnn \rightarrow \Sigma^0 \pi^0 \; n \; d$

$(K^- n) + ppn \rightarrow \Sigma^0 \pi^- \; p \; d$

- low energy (took away by the pion) not correlated Σ^0 d pairs.

It is easy to be disentangled (similar to the Σ^0 p analysis).